NMR Studies of the MgATP Binding Site of Adenylate Kinase and of a 45-Residue Peptide Fragment of the Enzyme†

David C. Fry,‡ Stephen A. Kuby,§ and Albert S. Mildvan*,‡

Department of Biological Chemistry, Johns Hopkins University School of Medicine, Baltimore, Maryland 21205, and Laboratory for the Study of Hereditary and Metabolic Disorders and Departments of Biological Chemistry and Medicine, University of Utah, Salt Lake City, Utah 84108

Received December 10, 1984

ABSTRACT: Proton NMR was used to study the interaction of β,γ-bidentate $Cr^{3+}ATP$ and MgATP with rabbit muscle adenylate kinase, which has 194 amino acids, and with a synthetic peptide consisting of residues 1–45 of the enzyme, which has previously been shown to bind MgϵATP [Hamada, M., Palmieri, R. H., Russell, G. A., & Kuby, S. A. (1979) *Arch. Biochem. Biophys. 195*, 155–177]. The peptide is globular and binds $Cr^{3+}ATP$ competitively with MgATP with a dissociation constant, $K_D(Cr^{3+}ATP)$ = 35 μM, comparable to that of the complete enzyme [$K_I(Cr^{3+}ATP)$ = 12 μM]. Time-dependent nuclear Overhauser effects (NOE's) were used to measure interproton distances on enzyme- and peptide-bound MgATP. The correlation time was measured directly for peptide-bound MgATP by studying the frequency dependence of the NOE's at 250 and 500 MHz. The H2′ to H1′ distance so obtained (3.07 Å) was within the range established by X-ray and model-building studies of nucleotides (2.9 ± 0.2 Å). Interproton distances yielded conformations of enzyme- and peptide-bound MgATP with indistinguishable *anti*-glycosyl torsional angles (χ = 63 ± 12°) and 3′-endo/O1′-endo ribose puckers (δ = 96 ± 12°). Enzyme- and peptide-bound MgATP molecules exhibited different C4′–C5′ torsional angles (γ) of 170° and 50°, respectively. Ten intermolecular NOE's from protons of the enzyme and four such NOE's from protons of the peptide to protons of bound MgATP were detected, which indicated proximity of the adenine ribose moiety to the same residues on both the enzyme and the peptide. Paramagnetic effects of β,γ-bidentate $Cr^{3+}ATP$ on the longitudinal relaxation rates of protons of the peptide provided a set of distances to the side chains of five residues, which allowed the location of the bound Cr^{3+} atom to be uniquely defined. Distances from enzyme-bound $Cr^{3+}ATP$ to the side chains of three residues of the protein agreed with those measured for the peptide. The mutual consistency of interproton and Cr^{3+} to proton distances obtained in metal–ATP complexes of both the enzyme and the peptide suggests that the conformation of the peptide is very similar to that of residues 1–45 of the enzyme. When this was assumed to be the case and when molecular models and a computer graphics system were used, MgATP could be fit into the X-ray structure of adenylate kinase in a unique manner such that all of the distances determined by NMR were accommodated. The adenine ribose moiety is bound in a hydrophobic pocket consisting of residues Ile-28, Val-29, His-36, Leu-37, and Leu-91, while the Mg^{2+}–triphosphate portion binds near Lys-21 and -27 and Gln-24. In this complex, the γ-phosphoryl group of MgATP is directed toward residues 172–194 which, in the form of a peptide, has previously been shown to bind ϵAMP [Hamada, M., Palmieri, R. A., Russell, G. A., & Kuby, S. A. (1979) *Arch. Biochem. Biophys. 195*, 155–177]. The MgATP-binding site determined by NMR is also consistent with the results of chemical modification and kinetic studies and with structural and sequence homologies among many nucleotide binding proteins.

Adenylate kinase catalyzes the reaction

$$MgATP + AMP \rightleftharpoons MgADP + ADP \quad (1)$$

Purification of the enzyme has been achieved from a wide variety of sources, including the muscle of rabbit (Noda & Kuby, 1957), pig (Heil et al., 1974), calf (Kuby et al., 1978), carp (Noda et al., 1975), and human (Kuby et al., 1982), as well as from liver mitochondria (Markland & Wadkins, 1966; Hamada et al., 1982), rat brain (Pradhan & Criss, 1976), bakers' yeast (Chin et al., 1967), and the serum of patients with Duchenne muscular dystrophy (Hamada et al., 1981). Kinetic studies of the enzyme (Rhoads & Lowenstein, 1968; Hamada & Kuby, 1978) have suggested the presence of two distinct substrate binding sites: the MgATP-binding site, which binds magnesium–nucleotide complexes, and the AMP-binding site, which binds only uncomplexed AMP and ADP. This model has been confirmed by ^{31}P NMR studies of the enzyme (Nageswara Rao et al., 1978; Vasavada et al., 1984). However, the location of the two binding sites within the tertiary structure of the enzyme remains an unresolved problem. The X-ray structure of porcine adenylate kinase has been reported (Sachsenheimer & Schulz, 1977), and AMP- and ATP-binding sites have been proposed (Pai et al., 1977). The location of these sites was based upon indirect evidence, since neither AMP nor MgATP bound to the adenylate kinase crystals. Salicylate, an inhibitor of the enzyme, did bind, and this region was designated the ATP-binding site. MnATP also bound to the crystals, in a different location, resulting in a small electron density which was assigned as the AMP-binding site. These assigned binding sites did not readily explain some of the data previously acquired on the enzyme. Both were relatively far removed from histidine residue 36, which had been shown by photoinactivation (Schirmer et al., 1970) and NMR studies (McDonald et al., 1975) to have a high prob-

† This work was supported by National Institutes of Health Grants AM28616 and AM07824 and National Science Foundation Grant PCM8219464.

‡ Johns Hopkins University School of Medicine.

§ University of Utah.

0006-2960/85/0424-4680$01.50/0

ability of being at the active site. Further NMR experiments, utilizing intermolecular nuclear Overhauser effects (NOE's) between the enzyme and bound MgATP, and distance determinations to Cr^{3+}ATP, based on paramagnetic effects on T_1, established that the adenine ring bound within ~5 Å of His-36, while the Cr^{3+} atom was 12.9 ± 1.0 Å away (Smith & Mildvan, 1982). The range of positions for bound MgATP which satisfied these constraints was not compatible with the proposed MgATP-binding site.

A reassessment of the nucleotide binding sites was also necessitated by the remarkable finding by Hamada et al. (1979) that two fragments from a tryptic digest of rabbit muscle adenylate kinase selectively bound magnesium 1,N^6-ethenoadenosine 5′-triphosphate (MgϵATP)[1] and ϵAMP, with affinities comparable to that of the intact enzyme. The ATP-binding fragment, consisting of residues 1–44, and the AMP-binding fragment, corresponding to residues 172–194, were located in regions of the molecule that differed from the binding sites proposed on the basis of the X-ray data. These fragments offered an attractive opportunity for extending the NMR studies of adenylate kinase by individually examining what appeared to be, essentially, the two isolated substrate binding sites. The small size of these fragments would allow resonances arising from specific residues to be more clearly identified in the NMR spectrum, leading to a more extensive description of the distance relationships between atoms of the binding site and those of the bound nucleotides.

In the present study, a synthetic peptide corresponding to the MgATP-binding fragment of rabbit muscle adenylate kinase (residues 1–45) is studied by a variety of NMR methods using a smaller synthetic peptide consisting of residues 31–45 to confirm resonance assignments. With the larger peptide, the paramagnetic effects of Cr^{3+}ATP on the T_1 of nearby protons, and the intermolecular NOE experiments with MgATP, are carried out in much greater detail; in addition, the conformation of bound MgATP on both the peptide and the complete enzyme are examined through intramolecular NOE's by using a strategy that has been applied successfully to other ATP-binding enzymes (Rosevear et al., 1983). The mutual consistency of the results obtained with the peptide and the enzyme yields a detailed and reasonably unique description of the MgATP-binding site of adenylate kinase, which is in agreement with existing structural data as well as amino acid sequence homologies of several ATP-binding proteins. Preliminary reports of this work have been published (Fry et al., 1984a,b).

Experimental Procedures

Materials. Adenylate kinase from rabbit muscle was prepared according to Kuby et al. (1978) and crystallized 3 times. β,γ-Bidentate Cr^{3+}ATP was prepared by method A of Dunaway-Mariano & Cleland (1980a). ATP, Tris, and DTT were purchased from Sigma. Chelex-100 (100–200 mesh) and Dowex H^+ 50W-X2 (100–200 mesh) were obtained from Bio-Rad. Sephadex G-25 (medium) was from Pharmacia. Collodion bags (M_r 10000 cutoff) were from Schleicher & Schuell. D_2O, NaOD, and CD_3COOD were from Stohler.

Peptide Synthesis. Suitably protected peptides corresponding to residues 1–45, and to residues 31–45, of the rabbit muscle adenylate kinase (Kuby et al., 1984) were synthesized by the Merrifield solid phase approach (Stewart & Young, 1969; Blossey & Neckers, 1975; Merrifield et al., 1982) on chloromethylated polystyrene resin (Bio-Rad SX-1, 1% cross-linked; 1.34 mequiv/g).

The extent of coupling and deprotection were monitored by the colorimetric ninhydrin-based procedure of Sarin et al. (1981) [cf. Kaiser et al. (1970)]. At residue 33, radioactive *N-tert*-butyloxycarbonyl[2-^{14}C]glycine (New England Nuclear) [synthesized by the *t*-Boc azide procedure of Schnabel (1967)] was introduced to provide a convenient label for subsequent purification and isolation. Peptides were removed from the solid support and partially deprotected by treatment of the peptide resin with hydrogen bromide and trifluoroacetic acid. Removal of the remaining protecting groups was accomplished by catalytic hydrogenation and by treatment with boron tris(trifluoroacetate) in trifluoroacetic acid (Pless & Bauer, 1973). Each peptide was then purified by gel filtration on Sephadex G-25 (fine) in 0.5 M HOAc and by ion-exchange chromatography on Dowex 50-X2. After treatment with 0.3 M 2-mercaptoethanol, it was applied to a 165 × 2.3 cm column of Sephadex G-50 and developed with 0.1 M NH_4HCO_3–1 mM 2-mercaptoethanol, pH 7.9, and the pooled sample lyophilized. Amino acid compositions yielded near stoichiometric ratios and sequencing after removal of the *N*-acetylmethionine, residue 1, with CNBr [cf. Kuby et al. (unpublished results) for the methodology applied to the CNBr reaction and for sequencing techniques] eliminated the possibility of truncated peptides. The sequence of each peptide (Table I) corresponded accordingly to that of residues 1–45, or of residues 31–45, of rabbit muscle adenylate kinase (Kuby et al., 1984).

A complete description of the synthesis of these fragments (residues 1–45 and 31–45) and of the carboxyl-terminal peptide corresponding to residues 172–194 of rabbit muscle adenylate kinase, together with some properties of these peptide fragments and of several other synthetic peptides, is in preparation (Kuby et al., unpublished results).

Methods. Adenylate kinase was stored frozen in 25 mM DTE, 25 mM EDTA, and 20.5% ammonium sulfate. Before use, the enzyme was equilibrated with Tris-HCl, pH 7.4 (1 mM), NaCl (150 mM), and DTT (0.1 mM) by passage through a Sephadex G-25 column. The enzyme was concentrated in collodion bags and was deuterated by lyophilization and redissolution into D_2O 2 times. Adenylate kinase activity was assayed by the coupled enzyme method of Kuby et al. (1978). The protein concentration was determined by absorbance at 280 nm using ϵ = 0.52 $(mg/mL)^{-1}$ $(cm)^{-1}$.

The peptides were stored at −70 °C as dry powders, and were dissolved directly into the sample buffer before use. They were deuterated by lyophilization and redissolution into D_2O 2 times. Their concentrations were determined by measuring the amount of ^{14}C radioactivity (see above) in a small aliquot and by measuring the concentration of binding sites for Cr^{3+}ATP in the case of peptide 1–45.

Cr^{3+}ATP was prepared immediately before use. Its concentration was determined by absorbance at 424 nm using ϵ = 24 mM^{-1} cm^{-1} (Cleland & Mildvan, 1979). It was deuterated by repeated D_2O dilution and concentration by rotatory evaporation at low temperature. Deuteration of all other compounds was accomplished by repeated lyophilization and dissolution in D_2O.

NMR Experiments. All NMR experiments were performed at 24 °C with samples in D_2O. For the proton NMR studies at 250 MHz, a Bruker WM-250 spectrometer with 16-bit A/D conversion was utilized. Spectra were acquired at 24 °C by using 90° pulses, quadrature phase detection, and 16-bit A/D

[1] Abbreviations: ϵATP, 1,N^6-ethenoadenosine 5′-triphosphate; DTE, dithioerythritol; DTT, dithiothreitol; EDTA, ethylenediaminetetraacetic acid; Tris-HCl, tris(hydroxymethyl)aminomethane hydrochloride; DSS, sodium 4,4-dimethyl-4-silapentanesulfonate; pH*, pH meter reading in ^2H_2O; A/D, analog to digital.

Table I: Chemical Shift and pK_a Data for the Protons of Rabbit Muscle Adenylate Kinase Peptide 1–45[a] and Paramagnetic Relaxation Rate Effects and Distances Measured from Peptide-Bound Cr^{3+}ATP

peak no.[b]	chemical shift[b] (ppm)	pK_a[c]	tentative assignment	$(1/T_{1p})_b$[d] (s^{-1})	distance from Cr^{3+}(Å)[e]
2	8.55	6.53	His C2H	19.1	12.9
1	8.62	6.53	His C2H	15.0	13.4
13	6.80	9.90	Tyr C3H, C5H	6.62	15.3
12	6.83	9.98	Tyr C3H, C5H	6.48	15.4
8	7.13	10.1	Tyr C2H, C6H	5.56	15.8
9	7.08	10.0	Tyr C2H, C6H	5.42	15.9
7	7.17	10.1	Tyr C2H, C6H	5.11	16.0
3	7.50	9.43	Lys NH_3[f]	3.76	16.9
29–31	1.71	9.60	Lys C$\beta,\gamma,\delta H_2$; Arg CγH_2	3.47	17.1
22	3.01	9.86	CH_2 (incl Lys CϵH_2)	3.28	17.2
6, 10, 11	7.27		Phe ring H; His C4H	2.88	17.6
28	1.80		Arg CβH_2; Leu CγH	2.82	17.7
17	4.01		Gly CαH_2; Ser βCH_2	2.80	17.7
25	2.31	4.80	Glu CγH_2; Gln CγH_2	2.76	17.8
32–34	1.42		Ala CβH_3; Leu CβH_2; Ile CγH_2	2.52	18.0
4, 5	7.35		Phe ring H	2.43	18.1
27	2.07		CH_2; Ile CβH	2.01	18.8
35	1.22		Thr CγH_3; Ile CγH_3; Leu CδH_3	1.94	18.8
15	4.30		CαH	1.84	19.0
18–20	3.71		Arg CαH	1.60	19.4
26	2.12		MetSCH_3	1.36	20.0
36	0.92		Ile CγH_3; Leu CδH_3	1.25	20.2
16	4.15		CαH	1.20	20.4
37	0.89		Val CγH_3; Ile CδH_3; Leu CδH_3	1.15	20.5
24	2.62		Met CγH_2; Asp CβH_2	0.79	21.9

[a] The peptide sequence is M[1]-E-E-K-L-K-K-A-K-I[10]-I-F-V-V-G-G-P-G-S-G[20]-K-G-T-Q-C-E-K-I-V-H[30]-K-Y-G-Y-T-H-L-S-T-G[40]-D-L-L-R-A[45]. [b] Peak numbers and chemical shifts correspond to the spectrum in Figure 3A, which was obtained at pH* 5.6. Chemical shifts are reported with respect to external DSS. [c] Determined from a pH-titration study. pK_a values were obtained from fits to the Hill equation, assuming $n = 1$. [d] Paramagnetic effects on the $1/T_1$ of peptide protons were obtained by titrating 1.2 mM peptide with Cr^{3+}ATP throughout a range of 0.001–1.0 equiv. Effects were corrected for outer-sphere contributions by displacement of Cr^{3+}ATP with 50 mM MgATP. Values were normalized by using eq 2, with $n = 0.8$ and $K_D = 35$ μM. The average errors in $(1/T_{1p})_b$ come from three sources, the $1/T_{1p}$ measurements (15%), the outer-sphere contribution (15%), and the effects of partial overlap of some of the resonances (10%) (Granot, 1982), yielding an average total error of 23.5% and a maximal total error of 55.9%. [e] Obtained from eq 4 and 5, with $\tau_c = 2.8 \times 10^{-10}$ s, as determined by measuring $1/T_{1p}$ of H_2O at four frequencies. From the total errors in $(1/T_{1p})_b$ and the 25% error in τ_c, the maximal error in r is 8.3% and the average error is 5.0%. [f] Partially exchanged. Assignment based on chemical shift and pK_a.

conversion. Chemical shifts were calculated with reference to external DSS.

In order to examine the frequency dependence of certain nuclear Overhauser effects, the peptide sample was studied at both 250 and 500 MHz. The measurements at 500 MHz were performed at the New England NMR Facility at Yale University on a Bruker WM-500 spectrometer using 32K data points and a spectral width of 5000 Hz, with all other parameters comparable to those used at 250 MHz. Free MgATP was also studied at both frequencies, in an identical sample except for the absence of peptide, by using the same instrument settings.

Enzyme samples contained 1 mM Tris-HCl, 0.1 mM DTT, and 150 mM NaCl, with concentrations of adenylate kinase ranging from 0.4 to 1.0 mM. Peptide samples contained 150 mM NaCl and peptide concentrations of 0.8–2.0 mM. NMR samples were generally 300–400 μL in volume. All solutions were pretreated with Chelex-100 to remove metal impurities. The pH of D_2O solutions (pH*) is reported as read directly from the pH meter. pH adjustments were made with NaOD and CD_3COOD.

In experiments with Cr^{3+}ATP, T_1 values of enzyme and peptide resonances were measured by the nonselective saturation–recovery method (Markley et al., 1971). Enzyme and peptide samples were maintained at pH* 5.6 to ensure the stability of the Cr^{3+}–nucleotide complex. CrATP, at pH* 5.6, was added to the samples in ≤5-μL aliquots as needed. MgATP, at pH* 5.6, was added in 1–20-μL aliquots in displacement experiments. Spectra were obtained with 8K data points, a spectral width of 2500 Hz, and 256–2048 transients for the enzyme and 128–256 transients for the peptide. Correlation times for Cr^{3+}–proton dipolar interactions were determined by measuring the paramagnetic effects of peptide-bound Cr^{3+}ATP on T_1 of water protons at 24.3, 100, 250, and 360 MHz, as previously described (Mildvan et al., 1980; Smith & Mildvan, 1982).

NOE experiments were performed at pH* 7.4–7.5, at MgATP/enzyme and MgATP/peptide ratios of 10/1 and 5/1 respectively. Spectra were collected with 16K data points, a spectral width of 2500 Hz, an acquisition time of 3.3 s, 16 transients for T_1 measurements, and 128–256 transients for NOE measurements. T_1 values were measured by the selective saturation–recovery method (Tropp & Redfield, 1981). NOE's were generated by alternately preirradiating on and off the resonances of interest, in blocks of 16 transients each, according to the sequence (Mildvan et al., 1983):

$$[[\text{RD-preirradiation } (t,\omega_1) - \text{observation pulse}]_{16}-[\text{RD-preirradiation } (t,\omega_{control}) - \text{observation pulse}]_{16}-[\text{RD-preirradiation } (t,\omega_2) - \text{observation pulse}]_{16}]_8$$

where t is the duration of the preirradiation pulse (0.1–3.0 s), ω_1 and ω_2 represent enzyme, peptide, or MgATP resonances, $\omega_{control}$ is a control frequency far removed from any proton resonances (9.7 ppm), and RD is a relaxation period, equal to 4.3 s with the enzyme and 15.7 s with the peptide. Preirradiation was accomplished by using the decoupler, with the power set at 35 and 30 dB below 0.2 W for the enzyme and peptide, respectively. For surveys in which intermolecular NOE's from the enzyme (or peptide) to MgATP were sought, the preirradiation time was set at 0.5 and 3.0 s for the enzyme and peptide, respectively. The preirradiation frequency was shifted through the entire enzyme or peptide spectrum at intervals of 0.03–0.1 ppm. NOE's were measured by subtracting control spectra ($\omega_{control}$) from experimental spectra (ω_1 or ω_2).

Results

NMR Spectra of Rabbit Muscle Adenylate Kinase and Peptide Fragments 1–45 and 31–45. The present NMR studies were performed on rabbit muscle adenylate kinase and a synthetic peptide representing the 45 N-terminal amino acid

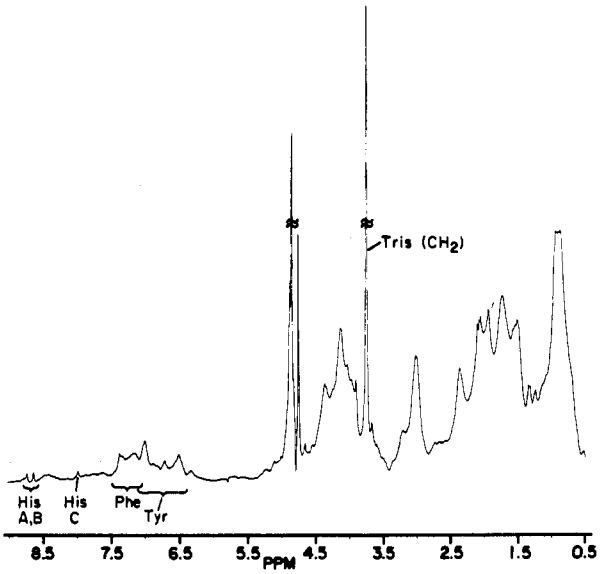

FIGURE 1: Proton NMR spectrum of rabbit muscle adenylate kinase. The sample contained 1.0 mM adenylate kinase in 150 mM NaCl, 1 mM Tris-HCl, and 0.1 mM DTT, pH* 5.5. Assignment of the peaks labeled A–C are described in the text. The spectrum was obtained at 250 MHz by using a 90° pulse, quadrature phase detection, 16-bit A/D conversion, 256 transients with 8K data points, a spectral width of 2500 Hz, an acquisition time of 1.6 s, a relaxation delay of 9.0 s, and T = 24 °C. Chemical shifts are given with reference to external DSS. The spectrum was processed with a 1.0-Hz line broadening.

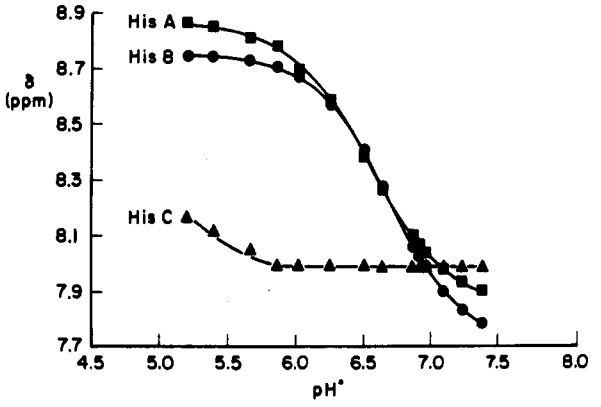

FIGURE 2: Titration curves depicting the effect of pH* on the chemical shifts of the histidine C-2 protons of rabbit muscle adenylate kinase. The sample contained 0.5 mM adenylate kinase, 150 mM NaCl, 1 mM Tris-HCl, and 0.1 mM DTT. pH* was adjusted with NaOD and CD_3COOD. The histidine C-2 resonances are labeled as in Figure 1, and their assignments are described in the text. Theoretical curves for histidines-A and -B were obtained by performing a least-squares fit to the Hill equation. The resulting parameters are as follows: histidine A, pK_a = 6.53, n = 1.47, δH° = 7.85 ppm, and δH^+ = 8.87 ppm; histidine B, pK_a = 6.69, n = 1.65, δH° = 7.72 ppm, and δH^+ = 8.75 ppm.

residues of this enzyme. A 250-MHz proton NMR spectrum of the enzyme is shown in Figure 1. Generalized assignments were made on the basis of chemical shifts (Wüthrich, 1976). The C-2 proton resonances of the three histidine residues of the enzyme (residues 30, 36, and 189 in the sequence) were separately resolved in the spectrum and labeled A–C. They were assigned by performing a pH titration, the results of which are given in Figure 2. It has been demonstrated that, of the two histidines present in calf muscle adenylate kinase (no. 36 and 189), only one, His-36, was titrable in the pH range 5–8 and exhibited a pK_a of 6.3 (McDonald et al., 1975). By analogy, the nontitrating resonance C of rabbit muscle adenylate kinase was designated His-189, and the two titrating resonances A and B represent His-36 and His-30. The pK_a

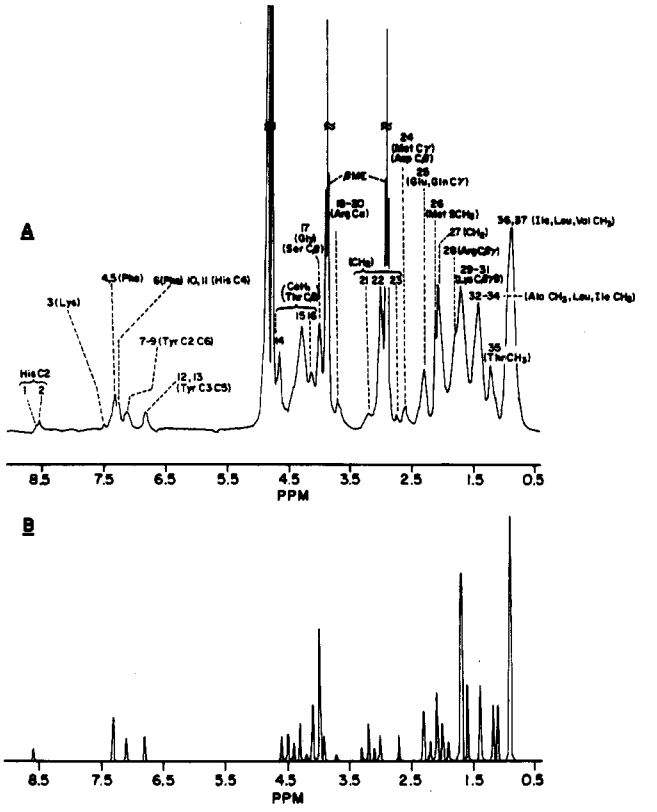

FIGURE 3: Proton NMR spectrum of the synthetic, residue 1–45, peptide fragment of rabbit muscle adenylate kinase (A). The peptide sequence and assignments are given in Table I. The sample contained 1.2 mM peptide in 150 mM NaCl and 40 mM β-mercaptoethanol, pH* 5.6. NMR conditions are as described in Figure 1. (B) Simulation of the spectrum of a random coil peptide of the same composition (Wüthrich, 1976).

of resonance A (6.5) is closer to that of His-36 in the porcine enzyme [6.3 (McDonald et al., 1975)] than is the pK_a of resonance B (6.7), suggesting that resonance A corresponds to His-36 and resonance B corresponds to His-30. This assignment is confirmed in a later section that shows an NOE from resonance A to adenine H-2 of bound MgATP as was found on the porcine enzyme for His-36 (Smith & Mildvan, 1982).

The spectrum of the 45 amino acid peptide was much more clearly resolved, as is shown in Figure 3A. The small shifts of the resonances from those expected for a random coil (Figure 3B), their broadness, with individual resonance widths ranging from 4.6 to 13.2 Hz, and their narrowing to values of 1.0–2.3 Hz upon denaturation of the peptide with 1.0 M acetone-d_6 (not shown) suggest that a globular tertiary structure is maintained by this fragment of the enzyme. The resonances of the peptide spectrum were assigned by chemical shift and by their behavior in a pH-titration study (Table I). The most unambiguous assignments were obtained for the aromatic region, since the peptide contains only one phenylalanine, two tyrosine, and two histidine residues. The histidine resonances were separate only at low pH and exhibited indistinguishable pK_a values (6.53) comparable to those found in the intact enzyme.

The validity of assigning resonances on the basis of chemical shift was demonstrated by studying a second synthetic peptide representing residues 31–45 of rabbit muscle adenylate kinase (Figure 4). In this smaller peptide, little shift or broadening of the resonances is seen and coupling is resolved, which suggest little higher order structure. The resonances could be almost completely assigned through the acquisition of

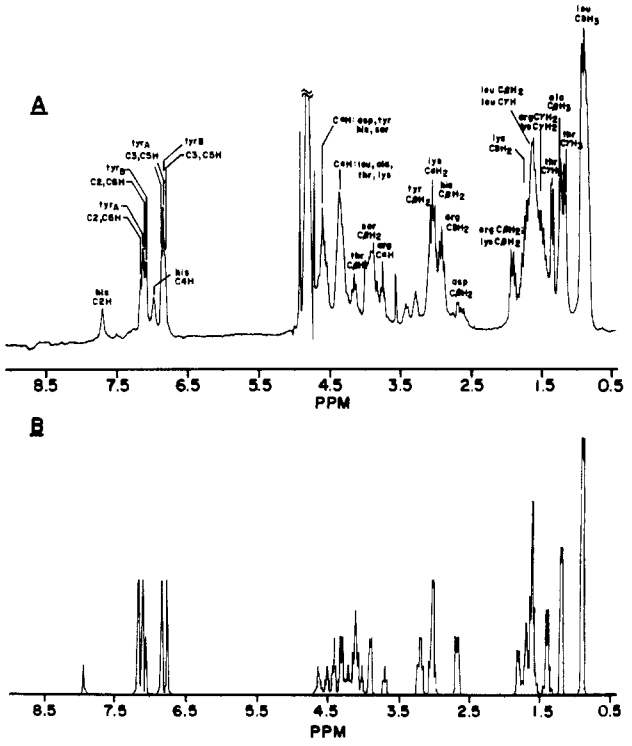

FIGURE 4: Proton NMR spectrum of the synthetic, residue 31–45, peptide fragment of rabbit muscle adenylate kinase (A). The peptide sequence and assignments are given in Table I. The sample contained 2.0 mM peptide in 150 mM NaCl, pH* 7.5. NMR conditions are as described in Figure 1, except that 512 transients with 16K data points, a 3.3-s acquisition time, and no relaxation delay were used here. (B) Simulation of the spectrum of a random-coil peptide of the same composition (Wüthrich, 1976).

two-dimensional correlated spectra (COSY). Alignment of spectra of the two peptides acquired under identical conditions showed that, for the portion of the larger peptide corresponding to residues 31–45, assignments had been made accurately. Also, it was apparent that resonances appearing only in the spectrum of the larger peptide had been correctly assigned to residues within the sequence 1–30 (Figure 3).

Binding of $Cr^{3+}ATP$ to Peptide 1–45. β,γ-Bidentate $Cr^{3+}ATP$, a competitive inhibitor of adenylate kinase with respect to MgATP (Dunaway-Mariano & Cleland, 1980b), was used as a paramagnetic probe of the ATP-binding sites of both the peptide and the enzyme. In experiments with the peptide, CrATP was titrated into the sample in numerous aliquots, ranging in size from 0.01 to 1.0 equiv. This allowed the paramagnetic effects on the longitudinal relaxation rates ($1/T_{1p}$) of all of the resonances to be monitored. Despite the multiplicity of the resonances, the saturation recovery graphs were not multiphasic within the time range used to determine $1/T_1$. For each resonance, a series of $1/T_{1p}$ values was obtained and used in the following equation (Gupta et al., 1976):

$$1/T_{1p\,obsd} = (1/T_{1p})_b[[([CrATP]_T + n[P]_T + K_D) - [([CrATP]_T + n[P]_T + K_D)^2 - 4([CrATP]_T n[P]_T)]^{1/2}]/2n[P]_T] \quad (2)$$

in which $(1/T_{1p})_b$ is the paramagnetic effect on the longitudinal relaxation rate caused by bound CrATP, $[P]_T$ and $[CrATP]_T$ are the total concentrations of peptide and CrATP, respectively, and n is the number of CrATP binding sites per peptide molecule. K_D, the dissociation constant of CrATP from the peptide, is defined as follows:

$$K_D = \frac{([CrATP]_T - [CrATP]_b)(n[P]_T - [CrATP]_b)}{[CrATP]_b} \quad (3)$$

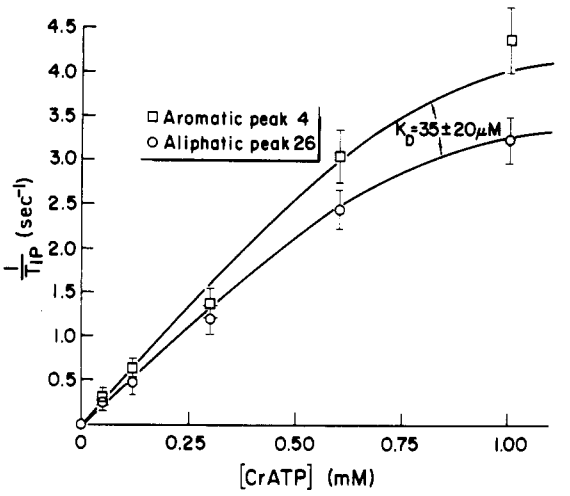

FIGURE 5: Titration curves showing the effect of added $Cr^{3+}ATP$ on the longitudinal relaxation rates of selected resonances of the peptide. Assignments of the peaks are given in Table I. The curves are theoretical least-squares fits to eq 2 using $n = 0.8$, $K_D = 35$ μM, and $(1/T_{1p})_b$ values as reported in Table I.

where $[CrATP]_b$ is the concentration of peptide-bound CrATP. Equations 2 and 3 were combined, and used in conjunction with a least-squares computer program, to find individual values of $(1/T_{1p})_b$ and values for n and K_D which best satisfied data from all of the resolved resonances, as exemplified by two cases in Figure 5. The binding stoichiometry thus determined ($n = 0.8 \pm 0.1$) is slightly less than unity, suggesting the partial loss of nucleotide binding sites, possibly due to denaturation. The value of K_D, 35 ± 20 μM, agreed well with the inhibitor constant (K_I) of CrATP with the complete enzyme (11.7 ± 0.7 μM), considering that the K_I was measured at a 30-fold lower ionic strength (Dunaway-Mariano & Cleland, 1980b).

Displacement of $Cr^{3+}ATP$ from the Peptide with MgATP. The contribution of outer-sphere effects to $(1/T_{1p})_b$ was determined by measuring the residual paramagnetic effects on $1/T_1$ after displacement of $Cr^{3+}ATP$ from the active site by excess MgATP. Depending on the observed resonance, maximal displacement by MgATP resulted in reductions of $(1/T_{1p})_b$ ranging from 50 to 87%, with an average of 70%. The concentration of MgATP (50 mM) which maximally displaced $Cr^{3+}ATP$ (1.0 mM) indicates that the dissociation constant of MgATP from the peptide is significantly lower than 1.8 mM. From kinetic studies of the intact enzyme, the K_m value of MgATP extrapolated to zero AMP levels is 20 μM (Hamada & Kuby, 1978).

Exchange Rate of $Cr^{3+}ATP$ on and off the Peptide. From the largest normalized $1/T_{2p}$ value of the peptide, that of aromatic peak 1, the rate constant for $Cr^{3+}ATP$ dissociating from the peptide, k_{off}, is estimated to be ≥544 ± 300 s^{-1}. This value is an order of magnitude greater than all of the $(1/T_{1p})_b$ rates, demonstrating no exchange limitation of $(1/T_{1p})_b$. Therefore, $(1/T_{1p})_b$ values, corrected for the outer-sphere contribution to the relaxation rate, may be used to determine the distance (r) between Cr^{3+} and the proton(s) of a given resonance. The lower limit value of k_{off} is comparable to the k_{cat} of the enzyme in the direction of MgATP formation (464 s^{-1}) (Hamada & Kuby, 1978). From the limiting value of k_{off} of $Cr^{3+}ATP$ and its dissociation constant, a lower limit to k_{on}, the rate constant for $Cr^{3+}ATP$ binding to the peptide, of ≥1.6 × 10^7 M^{-1} s^{-1} is estimated, which is well within the diffusion limit.

Calculation of Distances from $Cr^{3+}ATP$ to Protons of the Peptide. Since the $(1/T_{1p})_b$ values are not limited by chemical exchange, and the outer-sphere contributions have been

Table II: Chemical Shift and pK_a Data for Selected Protons of Rabbit Muscle Adenylate Kinase and Paramagnetic Relaxation Rate Effects and Distances Measured from Enzyme-Bound Cr^{3+}ATP

resonance (ppm)[a]	pK_a[b]	tentative assignment	$(1/T_{1p})_b$[c] (s^{-1})	distance from Cr^{3+} (Å)
3.24		Lys CϵH_2	59 ± 23	11.1 ± 1.0
8.71	6.5	His-A C2H	44 ± 19	11.8 ± 1.2
8.62	6.7	His-B C2H	27 ± 12	12.8 ± 1.5
7.95		His-C C2H	26 ± 12	12.8 ± 1.6
1.76		Lys Cγ,δH_2	26 ± 15	12.8 ± 1.9
6.71		Tyr C3H, C5H	17 ± 7	13.7 ± 0.9
6.51		Tyr C3H, C5H	17 ± 7	13.7 ± 0.9
3.05		Lys CϵH_2	14 ± 11	14.1 ± 4.0
7.15		Phe ring H	11 ± 4	14.8 ± 1.0

[a] Chemical shifts correspond to the spectrum in Figure 1, which was obtained at pH* 5.5, and are reported with respect to external DSS. [b] Determined from a pH-titration study covering a pH* range of 5.0–7.5; see Figure 2. [c] Paramagnetic effects on the $1/T_1$ of enzyme protons were obtained by titrating 0.84 mM enzyme with Cr^{3+}ATP throughout a range of 0.005–0.05 equiv. Values were normalized by using eq 2, assuming $n = 1.0$ and $K_D = 11$ μM. [d] Obtained from eq 4 and 5, with $\tau_c = 6.8 \times 10^{-10}$ s (Smith & Mildvan, 1982).

evaluated, these values may be used to calculate Cr^{3+} to proton distances with eq 4 (Mildvan & Gupta, 1978; Mildvan et al., 1980) where C is a constant, equal to 705 Å/$s^{1/3}$ for interactions between Cr^{3+} and protons. The correlation function, $f(\tau_c)$, is defined as follows:

$$r = C[(T_{1p})_b[f(\tau_c)]]^{1/6} \quad (4)$$

$$f(\tau_c) = \frac{3\tau_c}{1 + \omega_I^2\tau_c^2} + \frac{7\tau_c}{1 + \omega_s^2\tau_c^2} \quad (5)$$

where ω_I and ω_s are the nuclear and electron precession frequencies and τ_c is the correlation time. The correlation time was determined by measuring the $1/T_{1p}$ of water with samples of peptide with and without Cr^{3+}ATP, at four frequencies, as described under Experimental Procedures. This method has previously been shown to yield reliable estimates of τ_c (Mildvan et al., 1980). The final τ_c value, $(2.8 \pm 0.7) \times 10^{-10}$ s, represents an average of values obtained by assuming τ_c to be frequency independent and by using a least-squares-fitting computer program that allows the frequency dependence of τ_c to vary. Distances from the Cr^{3+} of Cr^{3+}ATP to peptide protons were obtained by using this value of τ_c and the $(1/T_{1p})_b$ measurements. A distance was calculated for each of the peptide resonances, and these are compiled in Table I.

Paramagnetic Effects of Cr^{3+}ATP on the Relaxation Rates of the Protons of Rabbit Muscle Adenylate Kinase. Adenylate kinase from rabbit muscle was found to be highly unstable in D_2O solution, exhibiting a loss of activity with a half-time of approximately 10 h. Hence, very limited titrations with Cr^{3+}ATP were conducted, typically with one or two additions of 0.005–0.05 equiv of the nucleotide, measuring paramagnetic effects on $1/T_1$ and $1/T_2$ of several resolved proton resonances (Table II). These experiments were terminated before a 60% loss of activity was reached. The largest $(1/T_{2p})_b$ value, 441 ± 100 s^{-1} for the C-2 proton of His-B (assigned to His-30), exceeded all $(1/T_{1p})_b$ values, indicating that the latter were not limited by the exchange rate of Cr^{3+}ATP. Complete displacement of Cr^{3+}ATP (0.005 equiv) from the active site of the enzyme by an excess of MgATP (2.4 equiv) was detected by the loss of paramagnetic effects on $1/T_1$ and $1/T_2$ of the C-2 proton resonance of His-A (assigned to His-36), indicating negligible outer-sphere contributions to the relaxation rates.

Distances from Cr^{3+}ATP to the resolved proton resonances were calculated from their $(1/T_{1p})_b$ values by using eq 4 with the correlation time of $(6.8 \pm 1.2) \times 10^{-10}$ s previously measured for the Cr^{3+}ATP complex of porcine muscle adenylate kinase by the frequency dependence of $1/T_{1p}$ of water protons (Smith & Mildvan, 1982). The $(1/T_{1p})_b$ value of His-A (assigned to His-36) yielded a Cr^{3+} to proton distance of 11.7 ± 2.0 Å, which agreed with those measured in other experiments (Table II) and with the Cr^{3+} to C-2 proton distance previously obtained (12.9 ± 1.0 Å) for His-36 of porcine adenylate kinase. Distances from the Cr^{3+} of Cr^{3+}ATP to several of the enzyme protons (Table II) indicate comparable proximity of the metal to both His-36 and His-30.

Studies of Conformation of Enzyme-Bound MgATP Using Nuclear Overhauser Effects. Nuclear Overhauser effects (NOE's) can be used to determine interproton distances of ≤4 Å (Noggle & Schirmer, 1971) and can, therefore, in fast exchanging systems yield information on the conformation of an enzyme-bound nucleotide (Karpeiski & Yakovlev, 1976; Rosevear et al., 1983), as well as proximities between protons of the bound nucleotide and those of the enzyme (or peptide) binding site (James, 1976; Bothner-By, 1979; Smith & Mildvan, 1982). Studies were conducted at [MgATP]/[peptide] and [MgATP]/[enzyme] ratios of 5/1 and 10/1, respectively. The enzyme exhibited a half-time for activity loss of about 36 h in the presence of this amount of MgATP. Intramolecular NOE's on bound MgATP were measured by selectivity preirradiating the H1′, H2′, H3′, H4′, H5′, and H8 protons and observing changes in the magnetization of the nonirradiated MgATP resonances. As exemplified in Figure 6A, the length of the preirradiation pulse was varied in order to obtain the time course of the development of the NOE's. This approach allows discrimination between primary and secondary effects, the latter of which will display a long lag period before development, and permits a more exact calculation of the cross-relaxation rate (σ) between the two protons using the equation (Wagner & Wüthrich, 1979):

$$f_A(B)_t = \frac{\sigma_{AB}}{\rho_A}(1 - e^{-\rho_A t}) + \frac{\sigma_{AB}}{\rho_A - c}(e^{-\rho_A t} - e^{-ct}) \quad (6)$$

In eq 6 $f_A(B)_t$ is the NOE to resonance A upon preirradiation of resonance B for t seconds, ρ_A is the longitudinal relaxation rate of resonance A, and c is the rate constant for saturation of resonance B. The cross-relaxation rate (σ_{AB}) can then be used to determine the distance (r_{AB}) between proton A and proton B according to the equation

$$r_{AB} = D[f(\tau_r)/\sigma_{AB}]^{1/6} \quad (7)$$

where D is a constant, $(\gamma^4\hbar^2/10)^{1/6}$, equal in this case to 62.02 Å/$s^{1/3}$, and $f(\tau_r)$ is a function of the correlation time (τ_r) such that

$$f(\tau_r) = \frac{6\tau_r}{1 + 4\omega_I^2\tau_r^2} - \tau_r \quad (8)$$

Intramolecular NOE's between protons of MgATP bound to the enzyme were negative. Time-dependent NOE data from pairs of protons were used in eq 6 to find best-fit values for σ, while also allowing c to vary. The determination of distances from measurements of σ requires the evaluation of τ_r, the correlation time for the interproton dipolar interaction. To evaluate τ_r, the distance between H2′ and H1′ was set at 2.9 Å. This distance has been shown by model-building studies to be relatively insensitive (±0.2 Å) to variations in ribose conformation and the glycosyl torsional angle (χ) (Rosevear et al., 1983). By use of the H2′–H1′ distance as a standard, values for τ_r of $(1.7 \pm 0.6) \times 10^{-9}$ s and for the correlation

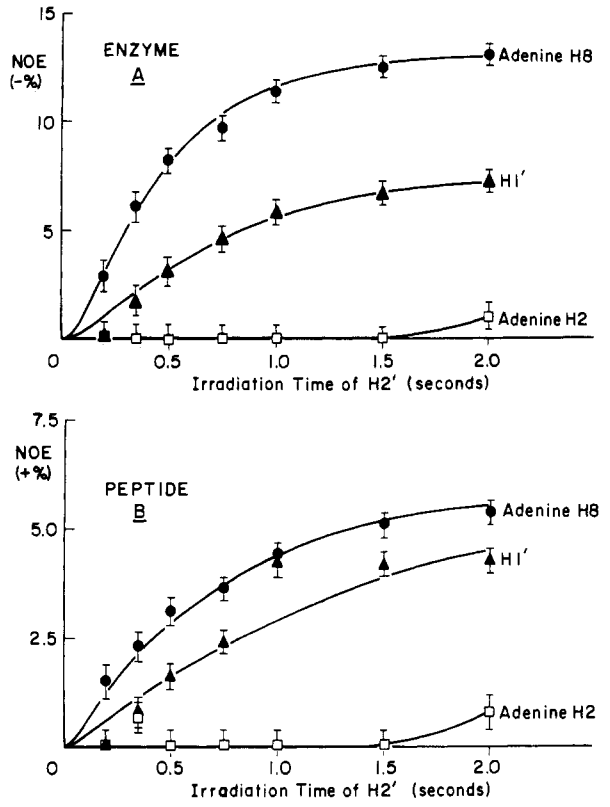

FIGURE 6: Time-dependent development of intramolecular NOE's to the H8, H2, and H1′ protons of MgATP bound to the enzyme (A) and the peptide (B) upon irradiation of H2′. In (A), the sample contained 0.6 mM adenylate kinase, 6.2 mM MgATP, 0.1 mM DTT, 150 mM NaCl, and 1 mM Tris-HCl, pH* 7.4 at 24 °C; in (B), the sample contained 1.0 mM peptide, 5.0 mM MgATP, and 150 mM NaCl, pH* 7.5 at 24 °C. Spectra were obtained at 250 MHz by using 90° pulse widths, quadrature phase detection, 16-bit A/D conversion, a spectral width of 2500 Hz, 16K data points per transient, an acquisition time of 3.3 s, and relaxation delays of 4.3 s in (A) and 15.7 s in (B); 128 transients were collected per spectrum in (A) and 256 in (B). The decoupler was used for preirradiation, with power set at 35 and 30 dB below 0.2 W in (A) and (B), respectively. The theoretical curves represent least-squares fits to eq 6.

function $f(\tau_r)$ of $(-1.3 \pm 0.7) \times 10^{-9}$ s were calculated from eq 7 and 8. This correlation function was then used to determine distances between the other pairs of protons, as reported in Table III. A model of ATP built utilizing these distances possessed an *anti*-glycosyl torsional angle, $\chi = 65 \pm 10°$, and a ribose pucker described by the angle $\delta = 102°$, indicating a ring exhibiting both 3′-endo and O1′-endo characteristics (Levitt & Warshel, 1978).

The single distance value determined from the NOE between the H5′ protons and that of H8 on enzyme-bound MgATP (Table III) does not uniquely identify the γ angle, which describes the orientation of O5′ relative to the ribose ring. Three such orientations have been found to be almost universally adopted by nucleotides, corresponding to those positions ($\gamma = 60 \pm 15°$, $180 \pm 10°$, and $300 \pm 20°$) in which all substituents about the C4′/C5′ bond are fully staggered (Saenger, 1984a,b). While the 60° conformation is excluded by the NOE, neither the 180° nor the 300° structure can be ruled out by this criterion. However, a γ value of 300° is unlikely since it has not been observed in nucleotides with 3′-endo ribose conformations (Saenger, 1984a,b). Moreover, positioning of the complete MgATP conformation into the X-ray structure of adenylate kinase (see Discussion) minimizes unfavorable contacts when γ is 170°, while serious van der Waals overlap is observed when γ is 300°.

Table III: Intramolecular NOE's and Interproton Distances on MgATP Bound to Adenylate Kinase and the MgATP-Binding Peptide (Residues 1–45)

	enzyme			peptide	
NOE[a]	σ[b]	r (Å)[c]	r (Å)[d]	σ[e]	r (Å)[f]
H2′–H1′	−0.125	2.90	3.07	0.045	3.07
H2′–H8	−0.422	2.37	2.51	0.080	2.79
H3′–H8	−0.318	2.48	2.63	0.053	2.99
H4′–H1′	−0.132	2.87	3.04	0.032	3.26
H5′–H8	−0.144	2.83	3.00	≤0.012	≥3.8
H8–H1′	≥−0.044	≥3.4	≥3.6	≤0.012	≥3.8
H1′–H8	≥−0.053	≥3.3	≥3.5	≤0.021	≥3.5

[a] NOE's were obtained by irradiating the first resonance in each listed pair and observing the effect on the second resonance. No significant effects were seen on adenine H2. [b] Obtained from the time dependence of NOE development using eq 6. ρ_A values for H8 and H1′ were 2.3 ± 0.3 and 1.3 ± 0.2 s^{-1}, respectively. Errors in σ are ±20%. [c] Obtained by using eq 7 and 8 with $\tau_r = 1.7 \times 10^{-9}$ s as calculated by setting the H2′–H1′ distance to 2.90 Å as a standard. Errors in r are ±8%. [d] Obtained by setting the H2′–H1′ distance to 3.07 Å as a standard. [e] Obtained at 250 MHz from the time dependence of NOE development using eq 6. ρ_A values are given in Table V. Errors in σ are ±20%. [f] Obtained by using eq 7 and 8 with $\tau_r = 2.3 \times 10^{-10}$ s as directly determined from the frequency dependence of σ (see Table V). Errors in r are ±8%.

Table IV: Intermolecular NOE's from Resonances of Adenylate Kinase and the MgATP-Binding Peptide (Residues 1–45) to Those of Bound MgATP[a]

NOE from enzyme		NOE from peptide		to (MgATP	
ppm	% NOE	ppm	% NOE	resonance)	probable identity[b]
0.9	−2.0			H8	Leu-91 CδH_3
1.2	−2.6	1.2	1.7	H8	Ile-28 CγH_3
1.5	−2.9			H8	Leu-91 CγH_3
2.0	−1.7	2.0	1.0	H8	Ile-28 CβH
1.1	−2.4	1.1	1.5	H2	Leu-37 CδH_3
1.8	−3.0	1.8	1.5	H2	Leu-37 CγH
7.9	−1.6	[c]		H2	His-36 C2H
0.3	−2.5			H1′	Leu-91 or -116 CδH_3
1.1	−3.5			H1′	Leu-91 CδH_3
1.6	−1.8			H1′	Leu-91 CβH

[a] NOE's were sought by irradiating the enzyme or peptide resonances at intervals of 0.03 to 0.1 ppm, as described in the text. Chemical shifts are reported at pH* 7.4 and pH* 7.5 for the enzyme and peptide, respectively, and represent the areas producing reproducible, maximal effects on the bound MgATP resonances. [b] Determined on the basis of chemical shift and model building, as described in the Discussion. [c] Could not be tested due to the proximity of the irradiated and observed resonances.

Nuclear Overhauser Effects from Enzyme Protons to Those of MgATP. Intermolecular NOE's between protons of rabbit muscle adenylate kinase and those of bound MgATP were sought by systematically preirradiating resonances of the enzyme spectrum at intervals of 0.03–0.1 ppm as described under Experimental Procedures. At the chosen preirradiation time of 0.5 s, only primary effects had been observed in the time-course studies. Areas of the enzyme spectrum that produced intermolecular NOE's are listed in Table IV, along with their possible identities. The magnitudes of these effects (1.1–4.7%) permit an approximate range of intermolecular proton–proton distances to be set at 2.6–4.0 Å by using the interproton distances of bound MgATP to calibrate the system. An NOE from His-A (7.91 ppm) but none from His-B (7.84 ppm) to adenine H-2 was observed, which supports the assignment of His-A to His-36, since a corresponding NOE from His-36 of porcine adenylate kinase to adenine H-2 of bound MgATP was previously found (Smith & Mildvan, 1982). By elimination, the His-B resonance of the rabbit muscle enzyme is assigned to His-30. The porcine and calf muscle enzymes have

Table V: Determination of τ_r from the Frequency Dependence of σ and ρ Measurements for Adenylate Kinase Peptide 1–45 and Peptide-Bound MgATP and for Free MgATP

sample	NOE	σ_{250MHz}[a] (s^{-1})	σ_{500MHz} (s^{-1})	$\sigma_{250MHz}/\sigma_{500MHz}$	τ_r[b] (s)	r[c] (Å)
peptide + MgATP	H2′ to H8	0.080	0.025	3.2	2.3×10^{-10}	2.79
	Ile CβH to H8	0.030	0.0088	3.4	2.4×10^{-10}	3.29
	Ile $C\gamma H_3$ to H8	0.031	0.0096	3.2	2.3×10^{-10}	3.27
	H2′ to H1′	0.045	≤0.015[d]	≥3.0	2.3×10^{-10}[e]	3.07
free MgATP	H2′ to H8	0.097	0.060	1.6	1.3×10^{-10}	2.61

sample	resonance	ρ_{250MHz}[f] (s^{-1})	ρ_{500MHz} (s^{-1})	$\rho_{250MHz}/\rho_{500MHz}$	τ_r[g] (s)
peptide + MgATP	H8	1.32	0.934	1.4	1.8×10^{-10}
	H2	0.304	0.204	1.5	2.2×10^{-10}
	H1′	0.540	0.373	1.5	1.8×10^{-10}
	Glu $C\gamma H_2$	3.50	1.68	2.0	6×10^{-10}
free MgATP	H8	0.699	0.565	1.2	1.2×10^{-10}
	H2	0.162	0.132	1.2	1.2×10^{-10}
	H1′	0.362	0.274	1.3	1.5×10^{-10}

[a] Errors in σ are ±20%. [b] Determined directly from the $\sigma_{250MHz}/\sigma_{500MHz}$ ratio by using eq 7 and 8. Errors in τ_r are ±13%. [c] Determined from eq 7 by using the corresponding τ_r values. Errors in r are ±8%. Distances based on NOE's from multiple peptide protons may represent averages. [d] NOE's to H1′ were too small to be measured accurately at 500 MHz. [e] Assumed equal to the value obtained from the H2′ to H8 NOE's. [f] Errors in ρ are ±10%. [g] Determined directly from the $\rho_{250MHz}/\rho_{500MHz}$ ratio by using eq 9.

a Gln residue at this position (Kuby et al., 1984).

Conformation of Peptide-Bound MgATP from Nuclear Overhauser Effects. NOE experiments were also performed using MgATP bound to the peptide. In this relatively low molecular weight complex, all observed NOE's were positive. Intramolecular NOE's on peptide-bound MgATP were measured as described for the enzyme–MgATP samples (Figure 6B). In order to calculate absolute distances from the measured values of σ, the correlation time was evaluated by the novel technique of examining the frequency dependence of σ. It can be seen from eq 7 that at two differing frequencies the value of σ will change directly with that of $f(\tau_r)$, since the distance between two protons (r_{AB}), and the constant D, will be unaffected by frequency. When eq 8 is utilized, the ratio of the $f(\tau_r)$ values at two different frequencies can provide a direct evaluation of τ_r. By use of this τ_r value, absolute distances can be obtained from all σ measurements. The frequency dependence of the NOE between H2′ and H8 of peptide-bound MgATP was studied at 250 and 500 MHz, as described under Experimental Procedures. This NOE, which was the largest observed at 250 MHz, could still be reasonably well measured at 500 MHz, even though its magnitude was reduced at the higher frequency. The ratio of the σ values obtained at the two frequencies (Table V) was used to calculate τ_r, which was found to equal $(2.3 \pm 0.3) \times 10^{-10}$ s. Similar values for τ_r were obtained by using ratios measured for two intermolecular NOE's from protons of the peptide to those of bound MgATP (Table V). The frequency dependence of the H2′–H8 NOE was also determined for free MgATP, in a duplicate sample which lacked peptide. The resulting ratio of σ values was distinctly different from that of the peptide–MgATP complex, leading to a smaller τ_r of $(1.3 \pm 0.4) \times 10^{-10}$ s for MgATP. This correlation time agrees well with that of MnATP, $(1.0 \pm 0.2) \times 10^{-10}$ s, determined by paramagnetic effects on T_1 of water protons (Sloan & Mildvan, 1976). The longer τ_r value of MgATP in the presence of the peptide provides independent evidence for the binding of MgATP to the peptide.

The longitudinal relaxation rate of a proton (ρ_A) should also exhibit a frequency dependence; if this rate is regulated solely by interaction with a second proton (B), the correlation time should be related to ρ_A in the following manner (Mildvan et al., 1983):

$$\rho_A = \left[\frac{D}{r_{AB}}\right]^6 \left[\tau_r + \frac{3\tau_r}{1 + \omega_I^2\tau_r^2} + \frac{6\tau_r}{1 + 4\omega_I^2\tau_r^2}\right] \quad (9)$$

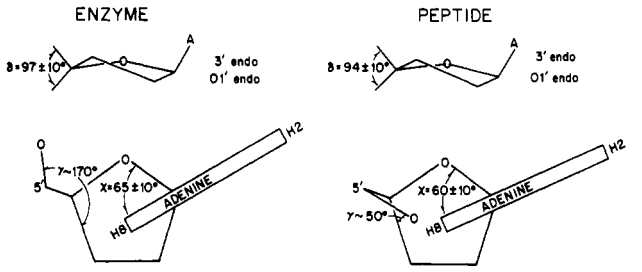

FIGURE 7: Conformation of bound MgATP on rabbit muscle adenylate kinase and on the MgATP-binding peptide. Conformations were determined by model building using the distances obtained from intramolecular NOE's, which are listed in Table III.

A ratio of ρ_A values at two different frequencies might then be used to calculate τ_r. The applicability of this approach was tested by using values obtained at 250 and 500 MHz for protons of the peptide, of peptide-bound MgATP, and of free MgATP. The results indicate an interproton τ_r for peptide-bound MgATP of $(1.9 \pm 0.3) \times 10^{-10}$ s, comparable to that found by frequency dependence of the σ values. The τ_r value of a peptide proton was significantly longer (Table V).

By use of the value of τ_r determined by the frequency dependence of σ, absolute distances were calculated from the intramolecular NOE data and are given in Table III. The H2′–H1′ distance was found to be 3.07 Å, which is within the range expected (2.9 ± 0.2 Å) from model-building and X-ray studies of nucleotides. A model of peptide-bound MgATP built by using the experimentally determined distances was found to possess an *anti*-glycosyl torsional angle, $\chi = 60 \pm 10°$, and a 3′-endo/O1′-endo sugar pucker, $\delta = 94 \pm 10°$. These conformational parameters overlap with those found for enzyme-bound MgATP (Table III). Reevaluation of the interproton distances on enzyme-bound MgATP by increasing the H2′–H1′ standard distance from 2.9 to 3.07 Å resulted in only a small decrease in the conformational angle δ describing the ribose pucker from 102° to 97° and no change in χ (Table III). Thus, no significant conformational differences are detected in the adenine–ribose regions of enzyme-bound and peptide–bound MgATP (Figure 7).

The only detectable difference between the enzyme- and peptide-bound conformations is in the C5′ to H8 distance, reflecting dissimilarity in the γ torsional angle, which describes the orientation of O5′ relative to the ribose ring. Of the three highly favored ranges of values for γ (Saenger, 1984a,b), only the range 60 ± 15° positions the H5′ protons far enough from H8 to preclude a measureable NOE between them, which is

apparently the case for peptide-bound MgATP.

Nuclear Overhauser Effects from Peptide Protons to Those of Bound MgATP. Intermolecular NOE's between protons of the peptide and those of bound MgATP were observed, providing direct evidence for the binding of MgATP by the peptide. These effects were positive and were quite small (1.0–1.9%), requiring preirradiation of ≥2.0 s for their detection. The pattern of intermolecular NOE's was compared to that obtained with the enzyme–MgATP complex, as is shown in Table IV. Tentative assignments of resonances of the enzyme and peptide which, upon irradiation, produced NOE's to resonances of MgATP were made on the basis of chemical shifts (Wüthrich, 1978) and model building (see Discussion).

One set of positive intramolecular NOE's was observed between resonances 22 and 29–31 of the peptide (Figure 3), yielding a distance of 2.61 ± 0.40 Å. This probably represents an effect between vicinal methylene protons of lysine.

Discussion

The goal of the present study was to define as fully as possible the ATP-binding site of adenylate kinase. This was accomplished by jointly considering NMR data obtained with the intact enzyme and the 45-residue ATP-binding peptide fragment. As will be described in detail, the peptide proved to adequately represent the isolated, functional ATP-binding site of adenylate kinase.

Although the smaller peptide corresponding to residues 31–45 provided a spectrum that could be almost fully assigned, it has not as yet been utilized in metal–ATP-binding studies because a peptide of such small size, with minimally shifted, narrow resonances and detectable coupling indicated a highly mobile structure. Moreover, it could not fully encompass the metal–ATP-binding site of the enzyme, since, as will be described, a substantial number of the residues (i.e., residues 21–30) found to participate in ATP binding are not present in the 31–45 peptide. Therefore, any adenylate kinase peptide fragment lacking residues 21–37, which comprises the region most obviously involved in metal–ATP binding, may not be as appropriate a model of the enzyme as peptide 1–45 is, even though such smaller peptides may show ATP-binding activity.

Binding of metal–ATP complexes to the peptide was supported by a variety of evidence. The binding of Cr^{3+}ATP was accompanied by paramagnetic effects on the $1/T_1$ and $1/T_2$ values of peptide resonances, which could be reversed by displacing Cr^{3+}ATP with MgATP. The stoichiometry, exchange rate, and K_D values measured for Cr^{3+}ATP binding to the peptide were reasonable and comparable to those obtained with the intact enzyme. Distances could be measured between Cr^{3+} and specific protons of the peptide, and these distances were all compatible with corresponding distances measured in the intact enzyme and, as will be discussed, with the X-ray structure of the enzyme. The binding of MgATP to the peptide was confirmed by the existence of intermolecular NOE's between protons of the peptide and those of the substrate. Also, peptide-bound MgATP possessed a correlation time significantly longer than that measured for free MgATP. Unlike the enzyme–ATPMg complex, the smaller peptide–ATPMg complex produced positive NOE's. Similarly, intramolecular NOE's between peptide protons were also positive, consistent with the small size of the complex. The observation that the peptide holds MgATP in a single conformation, almost indistinguishable from that found for MgATP bound to the enzyme, is further evidence of binding. At least three conformations were required to explain the NOE's observed with free $Co(NH_3)_4$ATP (Rosevear et al., 1983).

The conformation and location of the adenosine portion of bound MgATP was determined through the measurement of intramolecular and intermolecular NOE's. Values of σ obtained from these NOE's were used to calculate interproton distances, requiring the evaluation of the correlation time. For the peptide, the technique of measuring the frequency dependence of σ was shown to be a valid method for directly determining correlation times, since the H2′–H1′ MgATP interproton distance obtained in this manner agreed well with X-ray crystallographic (de Leeuw et al., 1980) and model-building studies (Rosevear et al., (1983). This technique should be applicable in any NOE study, providing the correlation time is of the correct magnitude for the frequencies available. For a comparison between 250 and 500 MHz, a suitable range for τ_r would be $(1–9) \times 10^{-10}$ s. The method should be particularly valuable in systems which lack an internal standard, i.e., an NOE-producing pair of nuclei, at an invariant distance apart. Even with a reference distance, measurement of σ at only one frequency, while suitable for calculating $f(\tau_r)$, hence interproton distances, occasionally yields ambiguous values of τ_r itself since eq 8 is a cubic with three roots. Although complicated by multiple interproton interactions, the frequency dependence of ρ may also be used to measure τ_r in diamagnetic systems. Thus, the ρ_{250}/ρ_{500} ratios of MgATP resonances gave consistent values of τ_r, comparable to those obtained by using the σ ratios (Table V). The ρ ratio measured for the Glu or Gln $C\gamma H_2$ resonance led to a larger τ_r value, probably due to more hindered motion of this residue.

The conformations of the adenine–ribose portion of MgATP bound to the enzyme and to the peptide, determined by model building using the calculated interproton distances (Table III), were found to agree within experimental error (Figure 7). This conformation, which possesses an *anti*-glycosyl torsional angle (χ = 60–65°) and a ribose pucker exhibiting both 3′-endo and O1′-endo character (δ = 94–97°), is consistent with structures derived from X-ray crystallographic studies (de Leeuw et al., 1980) and theoretical energy maps of purine ribonucleosides (Saenger, 1984a,b). The MgATP conformation on adenylate kinase is similar to but not identical with that found for the adenosine moiety of NAD bound to lactate dehydrogenase (3′-endo, χ = 84°) (Chandrasekhar et al., 1973), that of NADPH bound to dihydrofolate reductase (3′-endo, χ = 87°) (Matthews et al., 1979), and that of bound MgATP on protein kinase (O1′-endo, χ = 78°) (Rosevear et al., 1983).

The single difference between the enzyme- and peptide-bound conformations of MgATP was in the γ angle. The absence of an NOE between the H5′ protons and H8 on peptide-bound MgATP indicated that γ was 60 ± 15°, since this is the only value among those found to be predominantly adopted by nucleotides which separates H5′ far enough from H8 to prevent a visible NOE between them. The other γ angle most frequently observed for nucleotides with 3′-endo ribose pucker is 180 ± 10°, which is apparently that present in enzyme-bound MgATP, since this angle would produce an H5′–H8 NOE like that observed on the enzyme.

The distances from Cr^{3+}ATP and from the protons of MgATP to protons of the peptide were all considered in locating the MgATP-binding site of adenylate kinase. The three-dimensional structure of the peptide in solution, although demonstrated to be globular, could not be determined in detail by NMR studies. Therefore, to provide the simplest and potentially most relevant basis for comparison of information gained on the peptide and the enzyme, a model of the peptide was built in accordance with the X-ray structure of this portion

of the enzyme (Sachsenheimer & Schulz, 1977).[2] Positioning of MgATP within the X-ray structure of the enzyme was also aided by use of an Evans and Sutherland PS 300 computer graphics system, with which an ATP molecule could be independently manipulated in relation to the enzyme structure and distances to the enzyme monitored.

The metal complex of ATP was positioned within the tertiary structure by first determining where the Cr^{3+} atom of Cr^{3+}ATP was bound on the peptide. Of the many distances obtained from Cr^{3+} to protons of the peptide, only those involving uniquely assigned residues were utilized. The center of the ring of the single phenylalanine present (residue 12) was judged to be approximately 17.8 Å away from Cr^{3+} by averaging the distances obtained for its clearly identifiable aromatic proton resonances (Table I). The ring protons of the two tyrosines (residues 32 and 34) could not be specifically assigned, but the C3, C5 and C2, C6 proton pairs were found to produce equal average distances for both residues. Therefore, the Cr^{3+} atom was positioned accordingly, equidistant from the two tyrosine rings. The remaining two well-defined distances were from the histidine C-2 protons, which were assigned as previously described. Because the X-ray structure was based upon the porcine enzyme, the side chain of histidine-30 of the rabbit enzyme was built into the model by positioning its Cβ and Cγ atoms in correspondence to those of glutamine-30. Uncertainty introduced by this difference, or by misassignment of the histidine residues, is less than the errors in the measured distances and would not significantly effect the positioning of the Cr^{3+} atom. The five distances utilized were sufficient to localize the Cr^{3+} atom within a sphere 4 Å in diameter. Distances obtained for overlapping resonances with multiple identities are more difficult to interpret, but consistencies among $1/(fT_{1p})$ values of such resonances (Table I) indicate that the Cr^{3+} atom is relatively near one or more lysine residues and far from acetylmethionine (residue 1). Interestingly, these relationships, although not purposely built in, were observed in the model.

In the enzyme, distances to the Cr^{3+} of bound Cr^{3+}ATP were obtainable for only three uniquely assigned signals, the C-2 proton resonances of histidines-30, -36, and -189. By use of these three distances (Table II), the Cr^{3+} atom could be positioned less than 2 Å from the location established by using the peptide distances. Within error, therefore, the Cr^{3+} atom of Cr^{3+}ATP binds at the same place on both the peptide and the enzyme. Close proximity of Cr^{3+} to tyrosine and lysine residues, as observed in the peptide, was also indicated for the enzyme (Table II).

The conformation of bound MgATP (Figure 7), as determined by examining intramolecular NOE's (Table III), was helpful in accurately positioning the metal–ATP complex within the model. The position of the adenine–ribose moiety of bound MgATP was determined by attempting to satisfy all proximities based on the intermolecular NOE's seen between enzyme or peptide resonances and those of the substrate (Table IV). Intermolecular NOE's observed with the enzyme were measured at a preirradiation time of 0.5 s, a period during which one may assume only primary effects are produced and during which no secondary intramolecular NOE's were seen (Figure 6). Intermolecular NOE's to enzyme-bound MgATP are listed in Table IV; the possible identities of the enzyme resonances giving rise to these effects were made on the basis of chemical shift (Wüthrich, 1976) and their potential for proximity within 4 Å from a metal–ATP molecule anchored by the established Cr^{3+} position. Intermolecular NOE's from the peptide to bound MgATP were seen only after a 2-s preirradiation. This is probably because the effects were small and were only measureable when fully developed. It is unlikely that they were secondary effects, since NOE's seen with the peptide could be matched to unequivocally primary NOE's seen with the enzyme (Table IV). Because the histidine C-2H resonances are at most only 0.6 ppm from that of adenine H2, at the preirradiation times required with the peptide, any intermolecular NOE to H2 was overwhelmed by direct irradiation of H2 itself. For all of the other NOE's, exact identification was made by assuming that effects seen with the enzyme but not with the peptide were derived from protons present on residues 46–194 of the enzyme. Using these criteria and allowing small (<3 Å) changes in the positions of the flexible side-chains of Val-13, Gln-24, and Leu-37 from those found in the crystal structure, the adenine and ribose portions of ATP could be oriented within the model such that all of the proximities based on the intermolecular NOE's (Table IV) were accommodated.

Having established the positions of the adenine–ribose moiety of ATP and the Cr^{3+} atom, the different γ angles observed for peptide- and enzyme-bound MgATP were considered separately by setting each γ angle within the proper range and adjusting the triphosphate chain to minimize van der Waals overlaps. The Δ isomer of β,γ-bidentate Cr^{3+}ATP was assumed, since adenylate kinase shows a binding preference for this configuration (Dunaway-Mariano & Cleland, 1980b). Good fits were obtained by setting γ at 50° and 170° for the peptide- and enzyme-bound ATP molecules, respectively. Therefore, both γ angles could be accommodated within the X-ray structure of the enzyme by making minor changes in the triphosphate chain, without alteration in the positions of the Cr^{3+} atom or in the adenine and ribose rings, as shown in Figure 8. A MgATP molecule with a γ angle of 300° could not be fit into the enzyme without unacceptable overlap of the α-phosphoryl group with the backbone Cα and Cβ of Gln-24 and the amide carbonyl oxygen of Lys-21. Hence, this value of γ, which is not observed in X-ray structures of 3′-endo nucleotides (Saenger, 1984a,b), may be excluded.

The location of bound MgATP is well constrained by the position of Cr^{3+} at its phosphate end, by its own conformation, and by a set of 10 interproton NOE's from the peptide to the purine and ribose rings. The uncertainties in these constraints range from ±0.3 to ±1.9 Å, yielding a corresponding uncertainty of, at most, ±2 Å in the exact boundaries of the MgATP-binding site. Nevertheless, the site is well-defined with respect to the overall enzyme structure and is shown in Figures 9 and 10. The adenine ring is positioned within a hydrophobic pocket formed by the side chains of Ile-28, Val-29, Leu-91, Leu-37, and His-36. The ATP molecule is highly extended and cuts across the helix, bend, and strand of β-sheet formed by residues 23–37. Adenine H2 is near residues 36 and 37, and the α-, β-, and γ-phosphates are near the α-helix at the level of residue 23. The ribose ring is between the side chains of Gln-24 and Val-13, with its H1′–H4′ face directed away from the Gln residue. The $-NH_3^+$ group of lysine-21 and the side chain of Gln-24 can be positioned very close to

[2] In the enzyme the region composed of residues 90–94 is situated between two other strands of sequence corresponding to residues 35–38 and residues 10–14, which together form a parallel β-sheet. The peptide 1–45 lacks residues 90–94. Therefore, this sheet structure cannot be formed in a manner identical with that seen in the enzyme. The remaining two parallel β-strands may themselves combine to form a sheet structure. It was not found necessary to postulate such alterations in the backbone strucutre of the enzyme, as found by X-ray, in order to fit the distances obtained with the peptide by NMR.

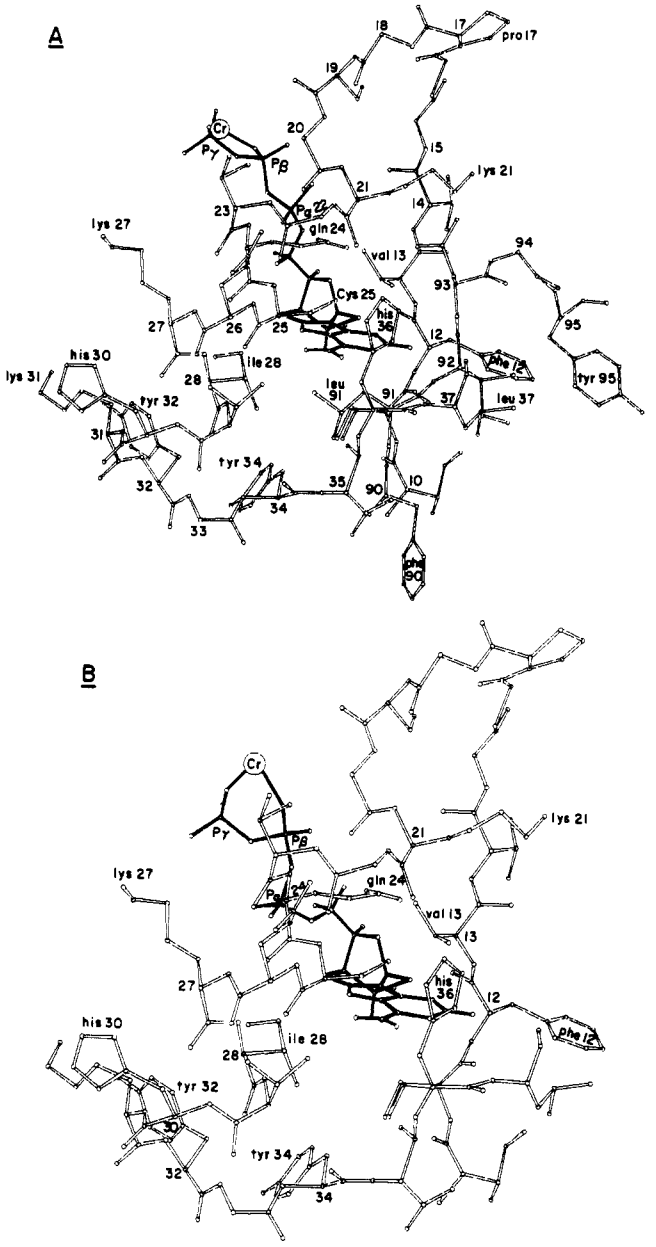

FIGURE 8: ORTEP drawings showing the MgATP-binding sites of adenylate kinase (A) and the 1–45-residue peptide (B). Enzyme and peptide structures were drawn by using the X-ray coordinates of Sachsenheimer & Schulz (1977). Residues 10–37 and 90–95 are shown in (A); residues 10–37 are shown in (B).

the α-phosphate, and Lys-27 can also closely approach the β- and γ-phosphates. Positioning the MgATP in this manner within the protein results in the orientation of its terminal phosphoryl group toward the strand of β-structure, β-turn, and α-helix formed by the carboxy-terminal 23 amino acid residues of adenylate kinase (Figure 10).[3] In accord with this finding, it was previously shown by Hamada et al. (1979) that a peptide corresponding to the carboxy-terminal 23 amino acids of adenylate kinase (residues 172–194) selectively binds ϵAMP with reasonable affinity. Thus, our model building based on distances measured in both the enzyme and the amino-terminal peptide makes a reasonable prediction as to the location of the other substrate, AMP.

[3] This location of the terminal phosphoryl group of MgATP is observed by using the conformational angle γ of MgATP found either on the peptide ($\sim$50°) or on the enzyme ($\sim$170°).

The ATP-binding site of adenylate kinase has features in common with nucleotide binding domains of other kinases and dehydrogenases such as the binding of the phosphate groups at the N-terminus of an α-helix (Chandrasekhar, et al., 1973; Hol, 1978) and the location of the adenosine moiety within a hydrophobic pocket near the side chains of Leu, Ile, Val, Ala, and occasionally His residues.

Our present conclusions are also consistent with homologies in the amino acid sequences of several ATP-binding proteins. It has been shown (Walker et al., 1982) that such ATPases as F_1, myosin, and rec A protein contain a homologous sequence eight residues in length, which is associated with the ATP-binding site. Several other proteins share this sequence (Table VI). Adenylate kinase also contains this sequence (Table VI; Figure 10) and exhibits a subsequent five-residue sequence that shows slight homology to the aforementioned proteins and strong homology to the ATP-binding regions of the cAMP- (Nelson et al., 1981) and cGMP- (Hashimoto et al., 1982) dependent protein kinase and to regions of other proteins. This includes rabbit muscle creatine kinase (Putney et al., 1984), whose reactive cysteinyl residue (no. 282) would correspond to Cys-25 of the rabbit muscle adenylate kinase. Also, note that an identical triplet of His-Leu-Ser appears in both adenylate kinase (residues 36–38) and in creatine kinase (residues 300–302) (Table VI). From the present work, adenylate kinase is the only protein, among those listed in Table VI, for which the ATP-binding site has been described in detail. The homologous regions, as shown by the stippling in Figure 10, are all found to be at or near the ATP-binding site. In adenylate kinase, residues with potential for direct interaction with ATP include Lys-21, Lys-27, Ile-28, and Val-29. Note that these, or analogous residues, are common to almost every protein considered. The function of the glycine-rich region preceding the common lysine is unknown. However, because its amino acid composition suggests that it should be highly flexible in solution, this area is proposed to be the locus of a conformational change, perhaps induced by substrate binding (Sachsenheimer & Schulz, 1977). Evidence suggesting such a change has been obtained for human (Kalbitzer et al., 1982) and yeast (Tomasselli & Noda, 1983) adenylate kinases and yeast hexokinase (Steitz et al., 1981). Conformational changes are also compatible with the functions of the other proteins that contain this sequence. In adenylate kinase, this flexible stretch of residues is located between the bound MgATP molecule and a large cleft extending to the surface of the enzyme (Figure 10). A conformational change in this region might alter the accessibility of this cleft or effect the orientation of Lys-21 toward the α-phosphate of bound MgATP.

The ATP-binding site of adenylate kinase (Figures 8–10) may be used to explain the results of chemical modification and kinetic studies. The present and previous NMR studies (Smith & Mildvan, 1982) indicate that His-36 may be directly involved in the binding of the adenine ring of ATP in accord with early photooxidation experiments (Schirmer, 1970). Studies with sulfhydryl modification reagents, such as 7-chloro-4-nitro-2,1,3-benzoxadiazole (Price, 1972), demonstrated that, of the two –SH groups present on the enzyme, one is highly reactive, near a lysine $-NH_2$ group, and is required for activity, though not for substrate binding. In the model, Cys-25, which is only $\sim$5 Å from the α-phosphate of bound ATP, could fit this description. Cys-25 is also one of the residues modified upon treatment of the enzyme with ferrate ion (Crivellone et al., 1985), a strongly oxidizing analogue of phosphate, which seems to react in a site-specific

Table VI: Sequence Homologies among the ATP-Binding Region of Adenylate Kinase and Segments of Other Proteins

	15	20	25	30	36	110	115	120
Adenylate kinase:[a]	G-G-P-G-S-G-K-G-T-Q-C-E-K-I-V-H-K-	/4/	-H-L-S	G-Q-P-T-L-L-L-Y-V-D-A-G				
F_1ATPase:[b]								
α(E. coli)	G-G- -G- -G-K-T-	-A-I-		G-	-A-L-I-I-Y-D-D-			
β(E. coli)	G-G- -G- -G-K-T-	-L-I-	-/4/-H-	G-	-V-L-L-F-V-D-			
β(bovine)	G-G- -G- -G-K-T-	-L-I-	-/4/-H-	G-Q-	-V-L-L-F-I-D-			
Myosin:								
nematode	G- -G- -G-K-T-	-K-V-I-						
rabbit	G- -G- -G-K-T-	-R-V-I-						
Rec A protein:	G- -S-G-K-T-T-	-V-I-						
Transducin α[c]	G- -G- -S-G-K- -T-	-K-						
G_o protein α[c]	G- -G- -S-G-K- -T-	-K-						
ras protein:[d]	G- -G[e] -G-K-	-L-I-		G-	-L-L-D-I-L-D-T-A[f]			
DNA A protein:[g]	G-G- -G- -G-K-T-	-V-						
Epstein-Barr virus protein:[h]	G-G- -G-K-G-	-A-						
Phospholipase A2:[i]	G- -G-G- -G-R-							
Protein kinase:[j]								
cAMP-dependent	G- -G- -G-R-	-/10/-K[k]-I-L-	-K					
cGMP-dependent		-K[k]-I-L-	-K					
src protein:	G- -G- -G-	-/10/-K[k]-T-L-K-						
Nitrogenase:[l]		-E-K-V-I-	-K					
Transcarboxylase biotin subunit:[m]	G-G- -G- -G-K-	-/10/-K-I-L-	-K			G-Q-T-V-L-V-L-E	-BCT-	
ATP/ADP Translocase:						G-	-V-L-V-L-Y-D	
Phosphofructokinase:						G-	-L-V-V-I-	-D-
Creatine kinase[n]	-G-	-C[o]-/9/-V-H-	-/3/-H-L-S				-L-L-L-	

[a] The sequence of rabbit muscle adenylate kinase is from Kuby et al. (1984). [b] Comparisons involving F_1-ATPases, myosin, rec A protein, ATP/ADP translocase, and phosphofructokinase are from Walker et al. (1982). /4/ represents an insert of four nonhomologous residues. [c] Partial sequences of the α-subunits of transducin from bovine retina and G_0 protein from bovine brain are from Hurley et al. (1984). [d] The sequence of a *ras* gene product is typified by that from the c-has/bas human protooncogene (Yuasa et al., 1983). Homologies involving this protein have been noted by Gay & Walker (1983). [e] Mutations at this position alter the transforming ability (Seeburg et al., 1984) and GTPase activity (Sweet et al., 1984) of the protein. [f] Substitution for a threonine at this position apparently results in autophosphorylation (McGrath et al., 1984). [g] Sequence from Hansen et al. (1982). [h] Sequence from Bankier et al. (1983). [i] Sequence from Joubert et al. (1981). [j] Sequences at the ATP-binding sites of the cAMP- and cGMP-dependent protein kinases were obtained from Hashimoto et al. (1982). Comparison of the cAMP-dependent protein kinase and $p60^{src}$, the transforming tyrosine kinase of Rous sarcoma virus, is from Kamps et al. (1984). /10/ represents an insert of 10 nonhomologous residues. [k] This lysine is the residue labeled during inactivation with 5′-[*p*-(fluorosulfonyl)benzoyl]adenosine (Kamps et al., 1984). [l] Sequence from Lammers et al. (1983). [m] Sequence from Maloy et al. (1979). /10/ represents an insert of 10 nonhomologous residues; BCT is the biocytin residue. [n] Sequence from Putney et al. (1984). /*n*/ represents an insert of *n* nonhomologous residues. [o] This cysteinyl residue is reactive with alkylating agents and is near the active site (Putney et al., 1984).

manner with phosphate-binding enzymes (Fajababu & Axelrod, 1978). The other residue modified by ferrate is Tyr-95, the side chain of which can be positioned ~7 Å from the α-phosphate group.

The hydrophobic pocket surrounding the adenine and ribose moieties of bound ATP appears spacious enough to accommodate a variety of ring structures, which may account for the relatively lower selectivity exhibit by this substrate site (Noda, 1973), including the low K_m and high forward V_{max} observed with $Mg\epsilon ATP^{2-}$ (Hamada & Kuby, 1978). The most sterically confined portion of bound ATP appears to be at the edge of the adenine ring near H2; this hydrogen is located near the peptide carbonyl groups of Leu-37 and Ile-92. The bulky C2 amino group of GTP and C2 carbonyl groups of CTP,

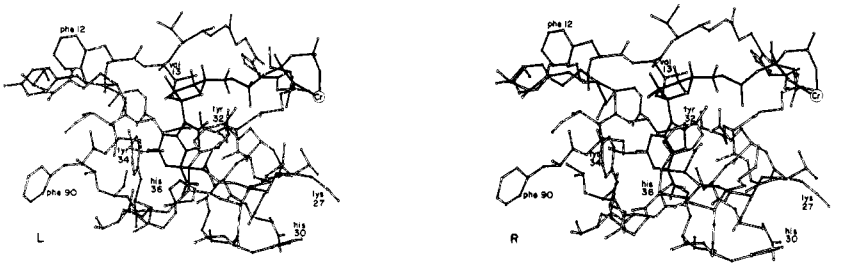

FIGURE 9: Stereo ORTEP drawing of the MgATP-binding site of adenylate kinase. Residues 10–37 and 90–95 are shown.

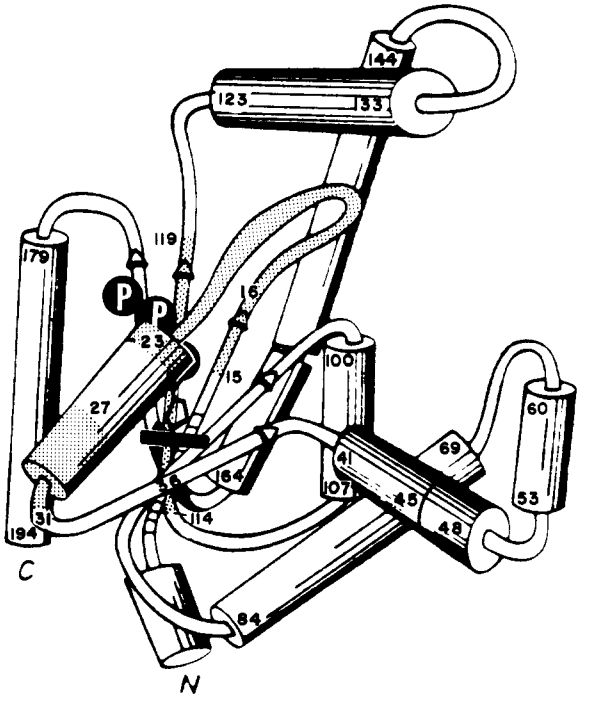

FIGURE 10: Simplified representation of the crystal structure of the entire adenylate kinase molecule showing the location of bound MgATP as determined by NMR. The orientation of the enzyme corresponds to that of Figure 8. Helices are indicated by cylinders and β-sheets by arrows. The strippled regions are areas that display sequence homology to other proteins (see Table VI). The enzyme structure was obtained from Pai et al. (1977).

UTP, and ITP may explain the order of magnitude higher K_m values of these substrates (O'Sullivan & Noda, 1968). The region with the least opportunity for specific enzyme–substrate contact is the ribose, probably explaining the low K_m and high forward V_{max} seen for $MgdATP^{2-}$, comparable to that found for ATP (O'Sullivan & Noda, 1968; Hamada & Kuby, 1978).

Our present data permit us to make reasonable suggestions as to the amino acid residues directly involved in catalysis. It was shown by Hamada et al. (1979) that a peptide corresponding to the carboxy-terminal 23 amino acids of adenylate kinase (residues 172–194) selectively binds ϵAMP with reasonable affinity, and our studies indicate that MgATP points toward this region. The reasonable assumption that the phosphate of AMP binds at the N-terminal end of an α-helix (Chandrasekhar et al., 1973; Hol et al., 1978) near a lysine yields the following orientation for bound AMP: its phosphate group would be bound near Lys-172, and its adenine ring would be situated in a hydrophobic area near Thr-188, His-189, Leu-190, and/or Val-186. Note that a Thr-His-Leu triplet (residues 35–37) also occurs at the ATP-binding site. This positioning of AMP would place its phosphate very close to the terminal phosphate of MgATP. The proposed reaction area would be flanked by residues 114–119 (Leu-Leu-Leu-Tyr-Val-Asp), a hydrophobic sequence conserved in several ATPases, in phosphofructokinase (Walker et al., 1982) and in creatine kinase (Putney et al., 1984) (Table VI). However, the fact that ATP/ADP translocase also has such a local sequence (Walker et al., 1982) implies its importance in binding and/or protecting the nucleotide from hydrolysis rather than in catalysis of phosphoryl transfer. In all of these systems this sequence is terminated by an aspartate residue which, in phosphofructokinase, is close to Mg^{2+}. Proximity to the Mg^{2+} of MgATP may be exhibited by Asp-119 of adenylate kinase, even though the enzyme appears to form an E–ATP–metal complex (Price et al., 1973), and there is no experimental evidence for a Mg^{2+} binding site on the enzyme (Kuby et al., 1962).

In conclusion, an ATP-binding site on adenylate kinase has been described which, on the basis of the crystal structure of the enzyme, successfully incorporates all of the distances obtained by NMR with the enzyme and the ATP-binding peptide in solution. This may not be the only site which can accommodate the data within the uncertainty limits of distance measurements and assignments, but it is the one that is derived from the fewest and simplest assumptions and that appears to best agree with kinetic and structural data and with sequence homologies among ATP-binding proteins.

ACKNOWLEDGMENTS

We are grateful to Eric Suchanek for help with the computer graphics system and to Terry Fox for skilled technical assistance.

REFERENCES

Bankier, A. T., Deininger, P. L., Farrell, P. J., & Barrell, B. G. (1983) *Mol. Biol. Med. 1*, 21–45.

Blossey, E. C., & Neckers, D. C. (1975) *Solid Phase Synthesis*, pp 1–360, Dowden, Hutchinson, and Ross, Stroudsburg, PA.

Bothner-By, A. (1979) in *Biological Applications of Magnetic Resonance* (Shulman, R. G., Ed.) pp 177–219, Academic Press, New York.

Chandrasekhar, K., McPherson, A., Adams, M. J., & Rossmann, M. G. (1973) *J. Mol. Biol. 76*, 503–519.

Chin, C. S., Su, S., & Russell, P. J. (1967) *Biochim. Biophys. Acta 132*, 361–369.

Cleland, W. W., & Mildvan, A. S. (1979) *Adv. Inorg. Biochem. 1*, 163–191.

Crivellone, M. D., Hermodson, M., & Axelrod, B. (1985) *J. Biol. Chem. 260*, 2657–2661.

de Leeuw, H. P. M., Haasnoot, C. A. G., & Altona, C. (1980) *Isr. J. Chem. 20*, 108–126.
Dunaway-Mariano, D., & Cleland, W. W. (1980a) *Biochemistry 19*, 1496–1505.
Dunaway-Mariano, D., & Cleland, W. W. (1980b) *Biochemistry 19*, 1506–1515.
Fry, D. C., Kuby, S. A., & Mildvan, A. S. (1984a) *Fed. Proc., Fed. Am. Soc. Exp. Biol. 43*, 1837.
Fry, D. C., Kuby, S. A., & Mildvan, A. S. (1984b) *Biochemistry 23*, 3357.
Gay, N. J., & Walker, J. E. (1983) *Nature (London) 301*, 262–264.
Granot, J. (1982) *J. Magn. Reson. 49*, 197–202.
Gupta, R. K., Fung, C. H., & Mildvan, A. S. (1976) *J. Biol. Chem. 251*, 2421–2430.
Hamada, M., & Kuby, S. A. (1978) *Arch. Biochem. Biophys. 190*, 772–792.
Hamada, M., Palmieri, R. H., Russell, G. A., & Kuby, S. A. (1979) *Arch. Biochem. Biophys. 195*, 155–177.
Hamada, M., Okuda, H., Oka, K., Watanabe, T., Veda, K., Nojima, M., Kuby, S. A., Manship, M., Tyler, F. H., & Ziter, F. A. (1981) *Biochim. Biophys. Acta 660*, 227–237.
Hamada, M., Sumida, M., Okuda, H., Watanabe, T., Nojima, M., & Kuby, S. A. (1982) *J. Biol. Chem. 257*, 13120–13128.
Hansen, E. B., Hansen, F. G., & von Meyenburg, K. (1982) *Nucleic Acids Res. 10*, 7373–7385.
Hashimoto, E., Takio, K., & Krebs, E. G. (1982) *J. Biol. Chem. 257*, 727–733.
Heil, A., Muller, G., Noda, L., Pinder, T., Schirmer, H., Schirmer, I., & Von Zabern, I. (1974) *Eur. J. Biochem. 43*, 131–144.
Hol, W. G. J., van Duynen, P. T., & Berendsen, H. J. C. (1978) *Nature (London) 273*, 443–446.
Hurley, J. B., Simon, M. I., Teplow, D. B., Robishaw, J. D., & Gilman, A. G. (1984) *Science (Washington, D.C.) 226*, 860–862.
James, T. L. (1976) *Biochemistry 15*, 4724–4730.
Joubert, F. J., & Haylett, T. (1981) *Hoppe-Seyler's Z Phys. Chem. 362*, 997–1006.
Kaiser, E., Colescott, R. L., Bossinger, C. D., & Cook, P. I. (1970) *Anal. Biochem. 34*, 595–598.
Kalbitzer, H. R., Marquetant, R., Rosch, P., & Schirmer, R. H. (1982) *Eur. J. Biochem. 126*, 531–536.
Kamps, M. P., Taylor, S. S., & Sefton, B. M. (1984) *Nature (London) 310*, 589–592.
Karpeiski, M. Y., & Yakovlev, G. I. (1976) *Bioorg. Khim. 2*, 1221–1230.
Kuby, S. A., Mahowald, T. A., & Noltmann, E. A. (1962) *Biochemistry 1*, 748–762.
Kuby, S. A., Hamada, M., Gerber, D., Tsai, W. C., Jacobs, H. K., Cress, M. C., Chua, S. K., Fleming, G., Wu, L. H., Fischer, A. H., Frischat, A., & Maland, L. (1978) *Arch. Biochem. Biophys. 187*, 34–52.
Kuby, S. A., Fleming, G., Frischat, A., Cress, M. C., & Hamada, M. (1982) *J. Biol. Chem. 258*, 1901–1907.
Kuby, S. A., Palmieri, R. H., Frischat, A., Fischer, A., H., Wu, L. H., Maland, L., & Manship, M. (1984) *Biochemistry 23*, 2393–2399.
Lammers, P. J., & Haselkorn, R. (1983) *Proc. Natl. Acad. Sci. U.S.A. 80*, 4723–4727.
Levitt, M., & Warshel, A. (1978) *J. Am. Chem. Soc. 100*, 2607–2613.
Maloy, W. L., Bowien, B. U., Zwolinski, G. K., Kumar, K. G., Wood, H. G., Ericsson, L. W., & Walsh, K. A. (1979) *J. Biol. Chem. 254*, 11615–11622.
Markland, F. S., & Wadkins, C. L. (1966) *J. Biol. Chem. 241*, 4124–4135.
Markley, J. L., Horsley, W. J., & Klein, M. P. (1971) *J. Chem. Phys. 55*, 3604–3605.
Matthews, D. A., Alden, R. A., Freer, S. T., Xuong, N. H., & Kraut, J. (1979) *J. Biol. Chem. 254*, 4144–4151.
McDonald, G. G., Cohn, M., & Noda, L. (1975) *J. Biol. Chem. 250*, 6947–6954.
McGrath, J. P., Capon, D. J., Goeddel, D. V., & Levinson, A. D. (1984) *Nature (London) 310*, 644–649.
Merrifield, R. B., Vizioli, L. D., & Boman, H. G. (1982) *Biochemistry 21*, 5020–5031.
Mildvan, A. S., & Gupta, R. (1978) *Methods Enzymol. 49G*, 322–359.
Mildvan, A. S., Granot, J., Smith, G. M., & Liebman, M. N. (1980) *Adv. Inorg. Biochem. 2*, 211–236.
Mildvan, A. S., Rosevear, P. R., Granot, J., O'Brian, C., Bramson, H. N., & Kaiser, E. T. (1983) *Methods Enzymol. 99*, 93–119.
Nageswara Rao, B. D., Cohn, M., & Noda, L. (1978) *J. Biol. Chem. 253*, 1149–1158.
Nelson, N. C., Zoeller, M. J., & Taylor, S. S. (1981) *Fed. Proc., Fed. Am. Soc. Exp. Biol. 40*, 1609.
Noda, L. (1973) *Enzymes, 3rd Ed. 8*, 279–305.
Noda, L., & Kuby, S. A. (1957) *J. Biol. Chem. 226*, 541–549.
Noda, L., Schulz, G. E., & Von Zabern, I. (1975) *Eur. J. Biochem. 51*, 229–235.
Noggle, J. H., & Schirmer, R. E. (1971) *The Nuclear Overhauser Effect*, pp 44–53, Academic Press, New York.
O'Sullivan, W. J., & Noda, L. (1968) *J. Biol. Chem. 243*, 1424–1433.
Pai, E. F., Sachsenheimer, W., Schirmer, R. H., & Schulz, G. E. (1977) *J. Mol. Biol. 114*, 37–45.
Pless, J., & Bauer, W. (1973) *Angew. Chem., Int. Ed. Engl. 12*, 147–148.
Pradhan, T. K., & Criss, W. E., (1976) *Enzymes, 3rd Ed. 21*, 327–331.
Price, N. C. (1972) *Fed. Proc., Fed. Am. Soc. Exp. Biol. 31*, 501.
Price, N. C., Reed, G. H., & Cohn, M. (1973) *Biochemistry 12*, 3322–3327.
Putney, S., Herlihy, W., Royal, N., Pang, H., Aposhian, H. V., Pickering, L., Belagage, R., Biemann, K., Page, D., Kuby, S. A., & Schimmel, P. (1984) *J. Biol. Chem. 259*, 14317–14320.
Rajababu, C., & Axelrod, B. (1978) *Arch. Biochem. Biophys. 188*, 31–36.
Rhoads, D. G., & Lowenstein, J. M. (1968) *J. Biol. Chem. 243*, 3963–3972.
Rosevear, P. R., Bramson, H. N., O'Brian, C., Kaiser, E. T., & Mildvan, A. S. (1983) *Biochemistry 22*, 3439–3447.
Sachsenheimer, W., & Schulz, G. E. (1977) *J. Mol. Biol. 114*, 23–36.
Saenger, W. (1984a) *Principles of Nucleic Acid Structure*, pp 9–80, Springer-Verlag, New York.
Saenger, W. (1984b) *Principles of Nucleic Acid Structure*, pp 385–413, Springer-Verlag, New York.
Sarin, V. K., Kent, S. B. H., Tam, J. P., & Merrifield, R. B. (1981) *Anal. Biochem. 117*, 147–157.
Schirmer, R. H., Schirmer, I., & Noda, L. (1970) *Biochim. Biophys. Acta 207*, 165–177.
Schnabel, E. (1967) *Justus Liebigs Ann. Chem. 702*, 188–196.
Seeburg, P. H., Colby, W. W., Capon, D. J., Goeddel, D. V., & Levinson, A. D. (1984) *Nature (London) 312*, 71–75.

Sloan, D. C., & Mildvan, A. S. (1976) *J. Biol. Chem. 251*, 2412-2420.
Smith, G. M., & Mildvan, A. S. (1982) *Biochemistry 21*, 6119-6123.
Steitz, T. A., Shoham, M., & Bennett, W. S. (1981) *Philos. Trans. R. Soc. London, Ser. B 293B*, 43-52.
Stewart, J. M., & Young, J. D. (1969) *Solid Phase Peptide Synthesis*, pp 1-103, W. H. Freeman, San Francisco.
Sweet, R. W., Yokoyama, S., Kamata, T., Feramisco, J. R., Rosenberg, M., & Gross, M. (1984) *Nature (London) 311*, 273-275.
Tomasselli, A. G., & Noda, L. (1983) *Eur. J. Biochem. 132*, 109-115.
Tropp, J., & Redfield, A. G. (1981) *Biochemistry 20*, 2133-2140.
Vasavada, K. V., Kaplan, J. I., & Nageswara Rao, B. D. (1984) *Biochemistry 23*, 961-968.
Wagner, G., & Wüthrich, K. (1979) *J. Magn. Reson. 33*, 675-680.
Walker, J. E., Saraste, M., Runswick, M. J., & Gay, N. J. (1982) *EMBO J. 1*, 945-951.
Wüthrich, K. (1976) *NMR in Biological Research: Peptides and Proteins*, pp 15-55, Elsevier Press, New York.
Yuasa, Y., Srivastava, S. K., Dunn, C. Y., Rhim, J. S., Reddy, E. P., & Aaronson, S. A. (1983) *Nature (London) 303*, 775-779.

Photoinactivation and Photoaffinity Labeling of Tryptophan Synthase $\alpha_2\beta_2$ Complex by the Product Analogue 6-Azido-L-tryptophan

Edith Wilson Miles*,‡ and Robert S. Phillips§

Laboratory of Biochemical Pharmacology and Laboratory of Chemistry, National Institute of Arthritis, Diabetes, and Digestive and Kidney Diseases, National Institutes of Health, Bethesda, Maryland 20205

Received January 14, 1985

ABSTRACT: The photoaffinity reagent 6-azido-L-tryptophan was synthesized by chemical methods. It binds reversibly in the dark to the $\alpha_2\beta_2$ complex of tryptophan synthase of *Escherichia coli* and forms a quinonoid intermediate with enzyme-bound pyridoxal phosphate (λ_{max} = 476 nm). The absorbance of this chromophore has been used for spectrophotometric titrations to determine the binding of 6-azido-L-tryptophan (the half-saturation value $[S]_{0.5}$ = 6.3 μM). Photolysis of the quinonoid form of the $\alpha_2\beta_2$ complex results in time-dependent inactivation of the β_2 subunit but not of the α subunit. The extent of photoinactivation is directly proportional to the absorbance at 476 nm of the quinonoid intermediate prior to photolysis. The substrate L-serine is a competitive inhibitor of 6-azido-L-tryptophan binding and photoinactivation. The competitive inhibitors L-tryptophan, D-tryptophan, and oxindolyl-L-alanine also protect against photoinactivation. The results demonstrate that 6-azido-L-tryptophan is a quasi-substrate for the $\alpha_2\beta_2$ complex of tryptophan synthase and that photolysis of the enzyme–quasi-substrate quinonoid intermediate results in photoinactivation. The modified $\alpha_2\beta_2$ complex retains its ability to bind pyridoxal phosphate and to cleave indole-3-glycerol phosphate, a reaction catalyzed by the α subunit. 6-Azido-L-tryptophan (side-chain 1,2,3-$^{14}C_3$ labeled) was synthesized enzymatically from 6-azidoindole and uniformly labeled L-[^{14}C]serine by the $\alpha_2\beta_2$ complex of tryptophan synthase on a preparative scale and has been isolated. Incorporation of ^{14}C label from 6-azido-L-[^{14}C]tryptophan is stoichiometric with inactivation. Our finding that most of the incorporated ^{14}C label is bound in an unstable linkage suggests that an active site carboxyl residue is the major site of photoaffinity labeling by 6-azido-L-tryptophan.

Tryptophan synthase $\alpha_2\beta_2$ complex (EC 4.1.2.20) from *Escherichia coli* catalyzes the synthesis of L-tryptophan from L-serine and indole-3-glycerol phosphate (reaction 1) or from L-serine and indole (reaction 2), as well as the cleavage of indole-3-glycerol phosphate (reaction 3). Reactions 2 and 3 are catalyzed at the active sites of the β_2 subunit and of the α subunit, respectively. [For reviews of tryptophan synthase, see Yanofsky & Crawford (1972) and Miles (1979).]

indole-3-glycerol phosphate + L-serine → L-tryptophan + D-glyceraldehyde 3-phosphate + H_2O (1)

indole + L-serine → L-tryptophan + H_2O (2)

indole-3-glycerol phosphate ⇌ indole + D-glyceraldehyde 3-phosphate (3)

Although the $\alpha_2\beta_2$ complex of tryptophan synthase does not catalyze degradation of L-tryptophan, it does bind L-tryptophan and forms a pyridoxal phosphate intermediate with L-tryptophan, which has an absorbance maximum at 476 nm (Miles, 1980; Tschopp & Kirschner, 1980; Lane & Kirschner, 1981; Tanizawa & Miles, 1983; Phillips et al., 1984). This intermediate probably has a quinonoid structure and results from removal of the α-proton of L-tryptophan from the Schiff-base intermediate. Similar quinonoid intermediates have been observed with oxindolyl-L-alanine and 2,3-dihydro-L-tryptophan, which are potent competitive inhibitors of the enzyme (Phillips et al., 1984). Tryptophan synthase catalyzes α-hydrogen exchange of L-tryptophan in ^2H_2O (Tsai et al., 1978; Miles, 1980) and of oxindolyl-L-alanine in ^3H_2O (Phillips et al., 1984).

Several active site residues have been previously identified in the β_2 subunit of tryptophan synthase. These include

‡ Laboratory of Biochemical Pharmacology.
§ Laboratory of Chemistry.